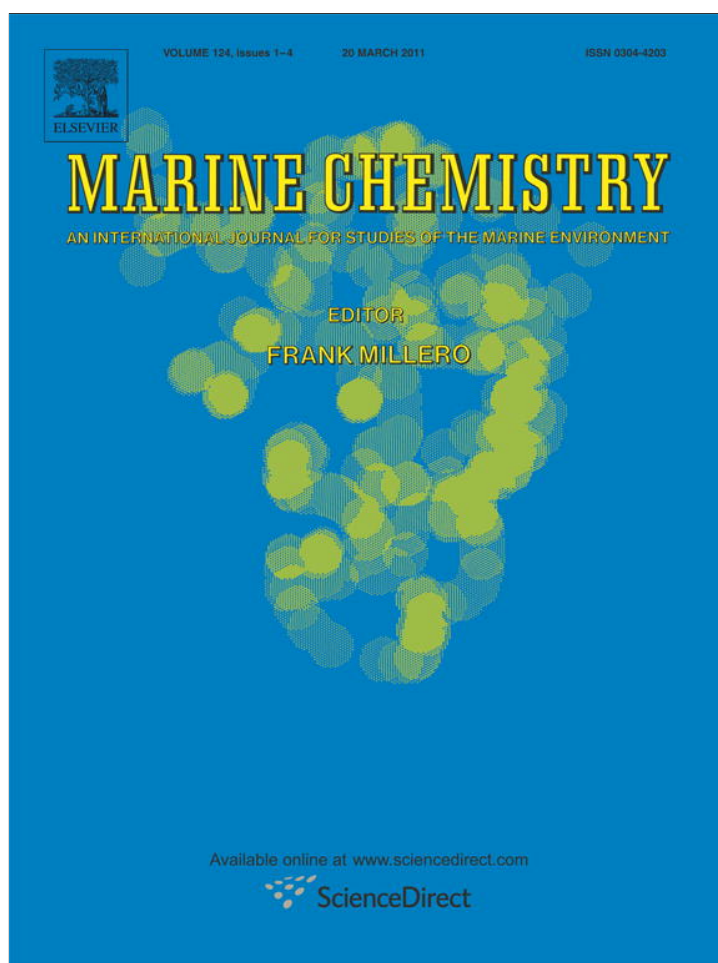


Provided for non-commercial research and education use.
Not for reproduction, distribution or commercial use.



This article appeared in a journal published by Elsevier. The attached copy is furnished to the author for internal non-commercial research and education use, including for instruction at the authors institution and sharing with colleagues.

Other uses, including reproduction and distribution, or selling or licensing copies, or posting to personal, institutional or third party websites are prohibited.

In most cases authors are permitted to post their version of the article (e.g. in Word or Tex form) to their personal website or institutional repository. Authors requiring further information regarding Elsevier's archiving and manuscript policies are encouraged to visit:

<http://www.elsevier.com/copyright>



Contents lists available at ScienceDirect

Marine Chemistry

journal homepage: www.elsevier.com/locate/marchem

Seasonal variability of dissolved inorganic carbon and surface water pCO₂ in the Scotian Shelf region of the Northwestern Atlantic

E.H. Shadwick^{a,*}, H. Thomas^a, K. Azetsu-Scott^b, B.J.W. Greenan^b, E. Head^b, E. Horne^b

^a Department of Oceanography, Dalhousie University, Halifax NS, Canada

^b Bedford Institute of Oceanography, Dartmouth NS, Canada

ARTICLE INFO

Article history:

Received 11 March 2010

Received in revised form 8 November 2010

Accepted 15 November 2010

Available online 25 November 2010

ABSTRACT

The seasonal variability of inorganic carbon in the surface waters of the Scotian Shelf region of the Canadian northwestern Atlantic Ocean was investigated. Seasonal variability was assessed using hourly measurements, covering a full annual cycle, of the partial pressure of CO₂ (pCO₂), and hydrographic variables obtained by an autonomous moored instrument (44.3°N and 63.3°W). These measurements were complemented by seasonal shipboard sampling of dissolved inorganic carbon (DIC), total alkalinity (TA), and pCO₂, at the mooring site, and over the larger spatial scale. Biological processes were found to be the dominant control on mixed-layer DIC, with the delivery of carbon-rich subsurface waters also playing an important role. Annual mixed-layer net community production was 2.4 mol C m⁻² yr⁻¹. The air–sea fluxes of CO₂ were computed using observed hourly wind speeds from the Sable Island Meteorological Station (43.9°N and 60.3°W). The region acts as a net source of CO₂ to the atmosphere on the annual scale ($F = -1.4 \text{ mol C m}^{-2} \text{ yr}^{-1}$), with a reversal of this trend occurring only during the spring phytoplankton bloom, when a pronounced undersaturation of the surface waters is reached for a short period. Outside of the spring bloom period, the competing effects of temperature and biology influence surface pCO₂ in roughly equal magnitude.

© 2010 Elsevier B.V. All rights reserved.

1. Introduction

The need to accurately balance the ocean carbon cycle is an important issue in current global climate research. Relative to their surface areas, the coastal oceans are the site of a disproportionately large fraction of ocean productivity (Cai et al., 2003; Borges et al., 2005). Although the coastal ocean represents only 8% of the total ocean surface area, roughly one-fifth to one-third of the global marine primary production takes place in these seas (Walsh, 1991). This productivity may be fueled by either terrestrial, atmospheric, or oceanic nutrient inputs, from natural or anthropogenic sources. High biological activity in coastal areas causes enhanced fluxes of CO₂ between the coastal ocean and the atmosphere, and also between coastal and open ocean environments (Thomas et al., 2004; Chen and Borges, 2009). Temporal variability in the coastal ocean is faster than in the open ocean environment. As such, the processes controlling the cycling of carbon in near-shore systems are difficult to resolve without continuous measurements of physical and biogeochemical variables. Sustained time-series measurements have done much to resolve uncertainties in carbon cycling for a number of coastal ocean regions (e.g., the North Sea, Belgian and Tasmanian coastal waters) (Bozec et al., 2006; Schiettecatte et al., 2006, 2007; Borges et al., 2008).

The North American Atlantic coast is fairly densely populated, and is therefore directly impacted by anthropogenic activities. However, baseline assessments of the carbon system, and the development of carbon budgets for these coastal regions have not yet been made (Najjar et al., 2010). A recent global synthesis of observational data from continental shelf regions suggests that temperate and high-latitude shelves largely act as sinks for atmospheric CO₂ (Chen and Borges, 2009). The Scotian Shelf is an open, temperate, continental shelf region. The Scotian Shelf is adjacent to the Gulf of Maine, and upstream from the South and Middle Atlantic Bights, three additional open continental shelf systems in both temperate and subtropical regions. Both the South (Jiang et al., 2008) and the Middle Atlantic Bight (Boehme et al., 1998; DeGrandpre et al., 2002) have been found to act as net sinks of atmospheric CO₂ in line with the synthesis of Chen and Borges (2009) and the most recent surface ocean CO₂ partial pressure (pCO₂) climatology of Takahashi et al. (2009). While outgassing is observed in summer, due to the warming of the surface waters and the corresponding increase in pCO₂, the South and Middle Atlantic Bights act as sinks for CO₂ in the autumn and winter seasons, in agreement with the classification of Chen and Borges (2009). Furthermore, in both the South and Middle Atlantic Bights, temperature is found to be the dominant control on the variability of pCO₂ over the annual cycle (DeGrandpre et al., 2002; Jiang et al., 2008). Modeling studies on the eastern North American continental shelf, including the Scotian Shelf and Gulf of Maine regions, have suggested that the region acts as an annual sink for atmospheric CO₂, and the

* Corresponding author. Tel.: +1 902 494 3670.

E-mail address: elizabeth.shadwick@dal.ca (E.H. Shadwick).

interannual variability in the air–sea CO_2 flux in this region is due in part to the North Atlantic Oscillation (Fennel et al., 2008; Previdi et al., 2009). We present the first observationally-based investigation of the inorganic carbon system in the Scotian Shelf region; this study emphasizes the utility of (long-term) time series measurements in the assessment of the carbonate system in coastal regions.

This study combined traditional ship-board sampling with autonomous time-series measurements to unravel the processes controlling the seasonal variability of carbon cycling in this coastal ocean environment. Hourly measurements covering a full annual cycle of the partial pressure of CO_2 ($p\text{CO}_2$), and hydrographic variables obtained by an autonomous moored instrument are presented. These measurements were complemented by spring and autumn ship-board sampling of dissolved inorganic carbon (DIC), total alkalinity (TA), and monthly sampling of hydrographic variables, at the mooring site. The controls on surface $p\text{CO}_2$ and DIC were investigated by isolating changes due to variations of temperature, as well as changes due to air–sea CO_2 flux, lateral and vertical transport, and biological production. A 1-D box model, using a conservation equation for DIC in the surface mixed-layer, was applied to quantify changes in DIC due to biological production throughout the year. Annual air–sea fluxes and mixed-layer net community production (NCP) were estimated.

2. Oceanographic setting

The Scotian Shelf is a highly productive area of the Canadian northwestern Atlantic Ocean (Fig. 1). This shelf region hosts active fisheries, is heavily influenced by river water input from the Gulf of St. Lawrence, and receives a downstream flow of water from the Labrador Sea. The Scotian Shelf has large temporal and spatial variations in its hydrographic properties as a result of its location downstream of the Gulf of St. Lawrence, and its unique position at the boundary of the North Atlantic sub-polar and subtropical gyres. The seasonal shelf-scale circulation on the Scotian Shelf is dominated by an equatorward flow, via the Nova Scotian current, on the inner shelf, and via an extension of the Labrador Current along the shelf edge (Hannah et al., 2001). The Nova Scotian current flows to the southwest, along the coast; transport varies seasonally in strength with peak values of 2 and 2.2 Sv in winter and spring, and a minimum of 0.4 Sv in summer (Loder et al., 2003). Smaller scale circulation

features include partial gyres generated by topographic steering around submarine banks (i.e. Browns Bank, Sable Island Bank, and Georges Bank), and cross-shelf channels (Loder et al., 1988; Hannah et al., 2001).

The dominant source of freshwater to the Scotian Shelf comes from the Gulf of St. Lawrence, via Cabot Strait. This freshwater input is on the order of $3 \times 10^{11} \text{ m}^3 \text{ yr}^{-1}$. For comparison, the Mississippi River discharges between 2 and $6 \times 10^{11} \text{ m}^3 \text{ yr}^{-1}$ (Penn, 2001), while the Sackville River at the mouth of Halifax Harbor discharges roughly $1.5 \times 10^8 \text{ m}^3 \text{ yr}^{-1}$ (Kepkay et al., 1997). The lowest salinities on the Scotian Shelf ($S < 31$) are found in the near-shore surface waters, while the deeper slope water has salinity of $S > 34$ (Petrie et al., 1987; Umoh and Thompson, 1994). There are significant seasonal variations in surface salinity, typically ranging near 1 unit of salinity (Loder et al., 1997), associated with the peak riverine discharge, delivered to the shelf between late June and early October. The region has a large range in seasonal sea-surface temperature (Fig. 2). In winter, surface temperatures are influenced by the equatorward, along-shelf, advection of subzero waters originating in Cabot Strait and the southern Newfoundland Shelf waters (Loder et al., 1997), and in summer the water warms to roughly 20°C . However, the short-term variation in temperature on the Scotian Shelf is primarily due to the contribution from the surface heat flux, with horizontal advection, mixing, and diffusion playing a minor role (Umoh and Thompson, 1994).

The origin and composition of water masses along the northeastern North American coast are well known (Bigelow, 1927; Hachey, 1942; Chapman and Beardsley, 1989; Loder et al., 1998). As many as eight distinct water masses have been identified on the Scotian Shelf on the basis of oxygen isotope and salinity data (Khatiwala et al., 1999; Houghton and Fairbanks, 2001). For simplicity, the water column in the region can be characterized by a two-layer system in winter when relatively fresh shelf water overlies more saline slope-derived water. In summer it is characterized by a three-layer system with the development of a warm, shallow, surface layer overlying the two-layer system (Loder et al., 1997). The Scotian Shelf region is influenced by tidal forcing, while episodic events, such as warm core rings entraining water off the shelf and flushing the deep basins, wind-driven coastal upwelling, and a meandering of the Nova Scotian current, are known to occur in the region (Petrie et al., 1987; Loder et al., 2003; Greenan et al., 2004). The analysis presented here employs a time-step of one month, with a

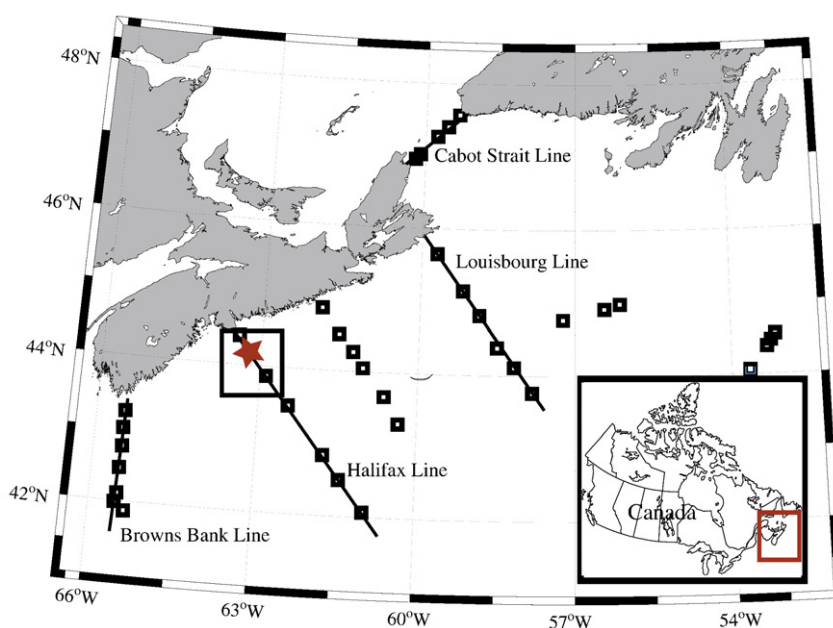


Fig. 1. Locations of stations sampled along four primary transect lines on the Scotian Shelf as part of the AZMP. Open squares indicate stations sampled on cruises in April 2007, April 2008, and September 2007. The location of station 'Halifax Line 2' (HL2) is indicated by the star.

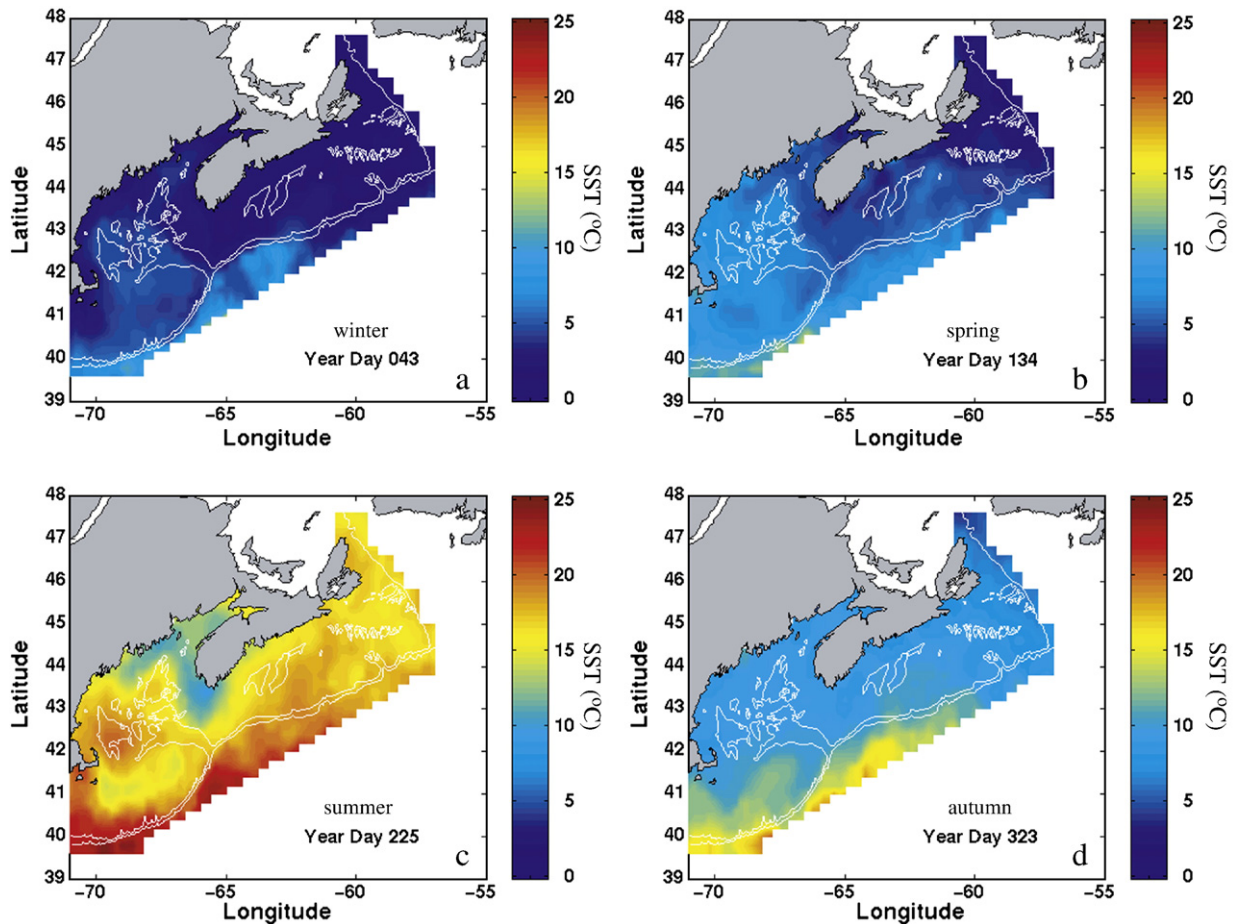


Fig. 2. Seasonal maps of sea-surface temperature ($^{\circ}\text{C}$) on the Scotian Shelf. The maps were generated from the data supplied by the Canadian Department of Fisheries and Oceans (Petrie et al., 1996).

seasonal focus, and therefore does not resolve these features. Furthermore, any net effect of short-term processes should be reflected in the monthly mean values, computed from higher resolution hourly data, applied here.

A climatology of hydrography, nutrients, and chlorophyll concentration in the region, based on historical archives from the Bedford Institute of Oceanography (B.I.O.) is given in Fig. 3. The data presented are for the Central Scotian Shelf (CSS) region ($43\text{--}45^{\circ}\text{N}$ and $62\text{--}64^{\circ}\text{W}$) and cover the period from 1930 to 2000. Monthly averages were computed for the parameters at the depths defined in Petrie et al. (1999). The size of this CSS box was chosen to provide robust monthly estimates of nutrients for which sampling is often sparse in the winter period. This climatology demonstrates the coincidence of spring bloom (in the chlorophyll-a record, Fig. 3 panel iv) and the nutrient depletion of the upper part of the water column (Fig. 3 panel iii) in this area of the continental shelf. The spring phytoplankton bloom makes a major contribution to total annual primary production in this region. This bloom propagates to the north along the Scotian Shelf at roughly 20 km day^{-1} , and can clearly be seen in satellite observations of ocean chlorophyll concentration (Siegel et al., 2002). The spring bloom on the Scotian Shelf is dominated by large phytoplankton size-classes and is terminated by the exhaustion of nitrate and silicate (Mousseau et al., 1996). The phytoplankton community is mainly comprised of diatom species, providing the main food source to planktonic animals and bottom-dwelling filter feeders. On the Scotian Shelf the spring bloom is the dominant control on phytoplankton biomass, though the more moderate summer production also plays a role (see Section 5.1). The spring bloom accounts for roughly one third of the total annual primary production on the Scotian Shelf which ranges from 60 to 130 g C m^{-2}

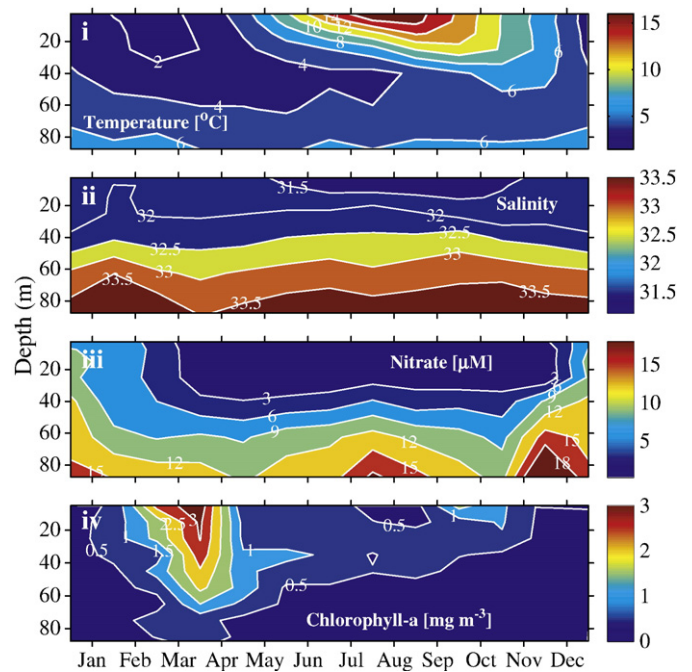


Fig. 3. A climatology of the central Scotian Shelf based on observations from B.I.O. archives. From top: (i) temperature [$^{\circ}\text{C}$], (ii) salinity, (iii) nitrate [μM] and (iv) chlorophyll-a concentration [mg Chl-a m^{-3}].

yr^{-1} (Fournier et al., 1977; Mills and Fournier, 1979). It represents the dominant source of primary productivity, setting the upper limit on organic matter export, production of higher trophic levels, and supply to benthic communities. During the remainder of the year, surface nitrate concentrations remain fairly low (Fig. 3 panel iii) and smaller sized phytoplankton dominate. The spring bloom occurs at the annual surface temperature minimum and is initiated by an increase in the amount of available light on the shelf (Greenan et al., 2004). Coastal upwelling in the Scotian Shelf region, caused by along-shore winds, drives the vertical and cross-shelf exchange of nutrient rich slope water, displacing nutrient depleted surface waters (Petrie et al., 1987). This process may contribute to the supply of nutrients required to support biological production in the region (Petrie et al., 1987; Greenan et al., 2004; Fennel et al., 2006).

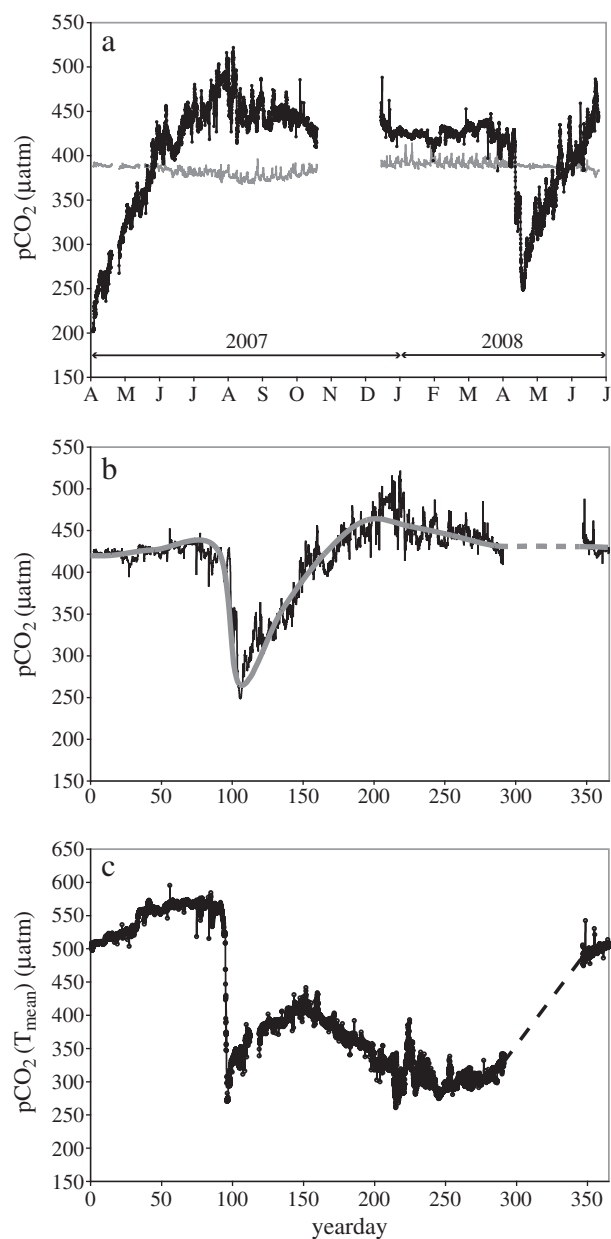


Fig. 4. (a) Hourly pCO_2 data measured by the CARIOCA buoy. The in-situ time series is given in black. The atmospheric CO_2 concentration measured at the nearby Sable Island station is given in gray. (b) An annual composite of surface water pCO_2 constructed from the time series shown in (a). The hourly data is given by the black line. The bold line is the (running) average over 14 days. (c) pCO_2 is normalized to the annual mean temperature (7°C) using the empirical relationship of Takahashi et al., (2002).

3. Data and methods

3.1. Sampling and analytical procedures

Hourly measurements of pCO_2 , salinity, sea surface temperature (SST), and chlorophyll-a (chl-a) fluorescence, were made using a CARIOCA-2 buoy (NKE, moored at station “Halifax Line 2”) (hereafter HL2) located at 44.3°N and 63.3°W , roughly 30 km offshore from Halifax, Nova Scotia (Figs. 1, 4 and 5). The pCO_2 measurements were made by an automated spectrophotometric technique which has been fully described elsewhere (Bates et al., 2000; Bakker et al., 2001; Bates et al., 2001; Hood and Merlivat, 2001). Data were uploaded and transmitted daily via the ARGOS satellite system. The CARIOCA was deployed from April to October 2007 and from mid-December 2007 to July 2008. From this time-series, the annual composite of surface water pCO_2 was constructed using observations from January to June 2008, from July to October 2007 and December 2007 (Fig. 4). A Sea-Bird (SBE 41) conductivity sensor and a Betatherm thermistor were used to acquire salinity and SST, while chl-a fluorescence was determined by a Wetlab miniature fluorometer (WETstar).

Chl-a fluorescence may be decreased by up to 80% during the day due to the effect of non-photochemical quenching, coincident with the strength of the incoming solar radiation (Kiefer, 1973). This effect is reduced by the application of strictly nighttime data during instrument calibration. Nighttime data were taken as a mean chl-a concentration between 0300 and 0600 UTC; data points were interpolated to match discrete chl-a measurements from ship-board occupations at HL2. A linear regression was used to determine the relationship between the CARIOCA fluorometer and discrete, measured chl-a values ($n = 29$, $r^2 = 0.76$, $p < 0.01$). This relationship was then applied to calibrate the CARIOCA chl-a time-series.

Discrete bottle samples were collected on two spring cruises and one autumn cruise as part of the Atlantic Zone Monitoring Program (AZMP) at stations distributed along four transects throughout the Scotian Shelf (Fig. 1). Cruises took place in April and September 2007, and April 2008. Approximately 350 samples were collected on each cruise from the entire water column with higher vertical resolution within the euphotic zone at all stations shown in Fig. 1. DIC and TA samples were collected from 20-L Niskin bottles mounted on a General Oceanic 24-bottle rosette fitted with a SeaBird CTD such that all chemical data are associated with high precision in-situ temperature, salinity and oxygen data. Following water collection, DIC and TA samples were poisoned with a solution of HgCl_2 to halt biological activity and stored in the dark at 4°C to await analysis. DIC and TA were analyzed by coulometric and potentiometric titration,

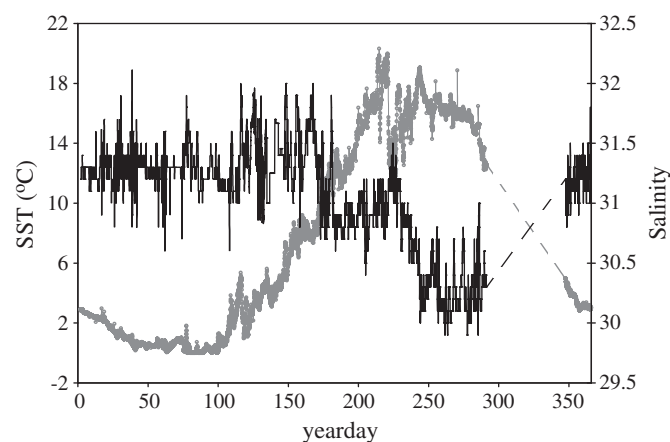


Fig. 5. An annual composite of surface salinity (black), and SST (gray) measured hourly by the CARIOCA buoy at station HL2. Salinity and SST data from occupations of HL2 in November and December confirm that the linear interpolation over the period when hourly observations are missing (dashed lines) is acceptable.

Table 1

The $p\text{CO}_2$ from the CARIOCA buoy is compared to $p\text{CO}_2^d$ computed from discrete samples of DIC and TA at station HL2. The values are given in units of μatm .

(dd/mm/yy)	$p\text{CO}_2(\text{CARIOCA})$	$p\text{CO}_2^d(\text{DIC, TA})$
12/04/07	203 ± 2	210 ± 5
02/05/07	327 ± 2	322 ± 5
10/08/07	443 ± 2	434 ± 5
18/10/07	418 ± 2	408 ± 5
06/04/08	424 ± 2	435 ± 5
14/04/08	249 ± 2	242 ± 5

respectively, using a VINDTA 3C (Versatile Instrument for the Determination of Titration Alkalinity by Marianda) (see for example Johnson et al., 1993, Fransson et al., 2001, or Bates et al., 2005 for a full description of the analytical methods for the determination of DIC and TA). Routine analysis of Certified Reference Materials (provided by A. G. Dickson, Scripps Institution of Oceanography) ensured that the uncertainty of the DIC and TA measurements was less than 2 to 3 $\mu\text{mol kg}^{-1}$, respectively. Following the determination of DIC and TA, discrete $p\text{CO}_2$ ($p\text{CO}_2^d = f(\text{DIC, TA})$), was computed using the standard set of carbonate system equations, excluding nutrients, with the CO_2Sys program of Lewis and Wallace (1998). We used the equilibrium constants of Mehrbach et al. (1973) refit by Dickson and Millero (1987). The calcium (Ca^{2+}) concentration was assumed to be conservative and calculated from salinity. A comparison of the CARIOCA $p\text{CO}_2$ and the (computed) discrete $p\text{CO}_2$ is given in Table 1. Additional hydrographic data, including profiles of temperature, salinity, and chl-a, were collected on monthly, or bimonthly, occupations of HL2.

A linear relationship between TA and salinity ($n = 784$, $r^2 = 0.92$, $p < 0.001$, standard error = $12 \mu\text{mol kg}^{-1}$, Fig. 6) was derived using samples collected on AZMP cruises throughout the whole water column at all stations in spring and autumn (Fig. 1):

$$\text{TA}_S = 43.2S + 805. \quad (1)$$

Eq. (1) was used to compute an annual cycle of surface TA concentration (Fig. 7a) at station HL2, using the hourly salinity data measured by the CARIOCA buoy at the same location (Fig. 5a). TA and $p\text{CO}_2$ were then used to compute the annual cycle of DIC (Fig. 7a)

using the CO_2Sys program (Lewis and Wallace, 1998) as described above.

The air–sea CO_2 flux (F) was computed using the conventional flux equation:

$$F = k\alpha\Delta p\text{CO}_2, \quad (2)$$

where k and α are the gas transfer velocity and solubility coefficient (Weiss, 1974) respectively, and $\Delta p\text{CO}_2$ is the gradient in $p\text{CO}_2$ between the ocean and the atmosphere. The gas transfer velocity, k , was computed using the formulation of Wanninkhof (1992) for short-term winds using observed hourly wind speed. Hourly wind speed was measured by Environment Canada at the Sable Island Meteorological Station (43.9°N and 60.3°W), at a height of 10 m. Petrie and Smith (1977) have shown that winds measured at Sable Island are representative of winds on the Scotian Shelf. Hourly atmospheric $p\text{CO}_2$ was also measured by Environment Canada at the Sable Island station. A negative flux indicates a transfer from the ocean into the atmosphere.

3.2. Application of a 1-D model

A diagnostic model was used to calculate the net change in DIC based on contributions from the processes controlling the variability of DIC in the surface mixed-layer allowing for the addition/removal of DIC from below. The following conservation equation, modified from Gruber et al. (1998), describes the changes in DIC in the mixed-layer:

$$\frac{d\text{DIC}}{dt} = \frac{F}{h} + \frac{1}{h}K_z \frac{d\text{DIC}}{dz} \Big|_{tc} + \frac{1}{h} \left(\frac{dK_x}{dx} \frac{d\text{DIC}}{dx} \right) + \frac{1}{h} \theta \left(\frac{dh}{dt} \right) (\text{DIC}_{tc} - \text{DIC}) + \text{Jtrsp} - \text{Jncp}, \quad (3)$$

where the terms on the right hand side of the equation represent, respectively, the contribution from (1) air–sea CO_2 flux, (2) vertical diffusion, (3) horizontal diffusion, (4) vertical entrainment, (5) a source term for horizontal advection, and (6) a source term for biological processes with the subscript ‘ncp’ referring to net community production. The variable mixed-layer depth is denoted h (m), K_z ($\text{m}^2 \text{s}^{-1}$) is the vertical diffusivity at the base of the mixed-

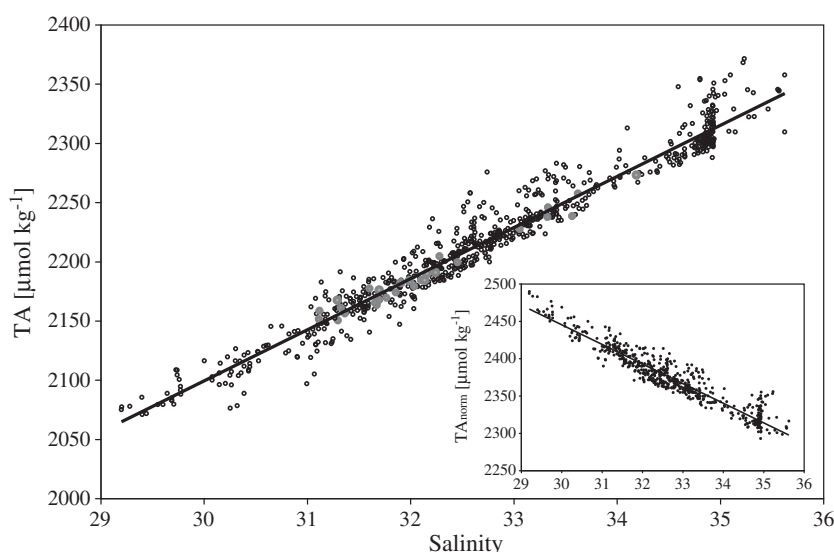


Fig. 6. TA and salinity data obtained from discrete samples collected on seasonal cruises in April and September throughout the Scotian Shelf at all stations shown in Fig. 1. All TA samples from the entire water column, collected on both the spring and autumn cruises are plotted. A linear regression yielded the following equation, $\text{TA} = 43.14S + 805$ ($n = 784$, $r^2 = 0.92$, $p < 0.001$, standard error = $12 \mu\text{mol kg}^{-1}$). Data from station HL2 are plotted in gray, and justify the use of the given linear relationship between TA and salinity at this location to compute the annual cycle of TA shown in Fig. 7a. Inset: TA normalized to a constant salinity ($\text{TA}_{\text{norm}} = 35\text{TA}/S$).

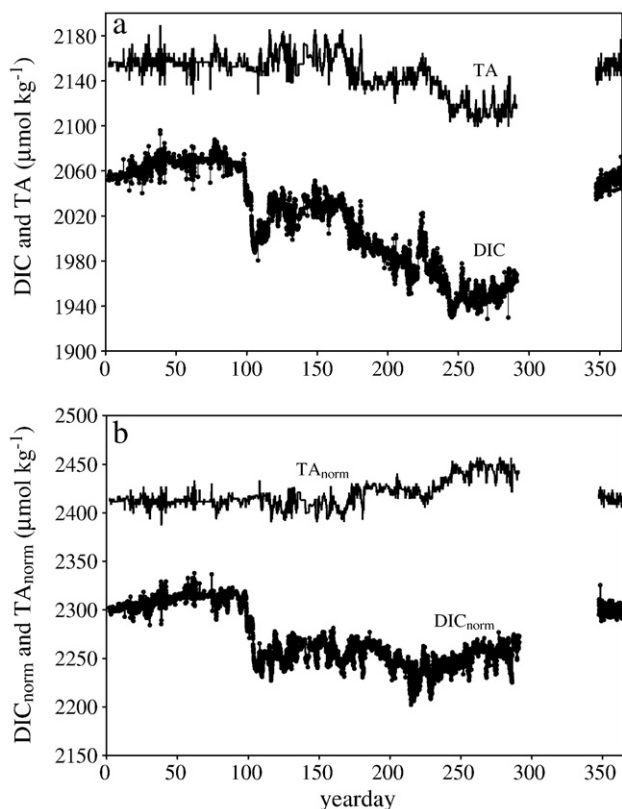


Fig. 7. (a) Annual cycles of hourly surface TA and DIC concentrations. TA was computed from the hourly CARIOCA salinity data, and the linear relationship between salinity and TA for the region (shown in Fig. 6). DIC was computed using the pCO₂ time-series from the CARIOCA and the annual cycle of TA. (b) Annual cycles of hourly salinity-normalized surface TA (TA_{norm}) and DIC (DIC_{norm} = 35DIC / S) concentrations.

layer, $dDIC/dz|_{tc}$ ($\mu\text{mol kg}^{-1} \text{m}^{-1}$) is the vertical gradient of DIC at the base of the mixed-layer, K_x ($\text{m}^2 \text{s}^{-1}$) is the horizontal diffusivity, $dDIC/dx$ ($\mu\text{mol kg}^{-1} \text{m}^{-1}$) is the horizontal gradient in DIC, DIC_{tc} ($\mu\text{mol kg}^{-1}$) is the DIC concentration in the thermocline (tc), below the mixed-layer. The Heaviside function, $\Theta = \Theta(\text{dh}/\text{dt})$ insures that shoaling of the mixed-layer (when $(\text{dh}/\text{dt}) < 0$) does not introduce new water into the mixed-layer, and only a deepening of the mixed-layer introduces water from the underlying layer. The horizontal diffusion term is assumed small, and any contribution should be accounted for in the J_{trsp} term. Measurements of surface DIC in April and September indicate that the gradient between two stations on the same transect line (Fig. 1) is roughly $30 \mu\text{mol kg}^{-1}$ over roughly $2.2 \times 10^4 \text{ m}$, or $1.4 \times 10^{-3} \mu\text{mol kg}^{-1} \text{m}^{-1}$. The gradient between surface DIC along the Halifax and along the Louisbourg Line (Fig. 1) is roughly $50 \mu\text{mol kg}^{-1}$ over $2.6 \times 10^5 \text{ m}$, or $1.9 \times 10^{-4} \mu\text{mol kg}^{-1} \text{m}^{-1}$. In the subsequent analysis, the contributions from both horizontal and vertical diffusion are included in the estimate of J_{trsp} (i.e. $J_{trsp} = V.\text{Diff} + H.\text{Diff} + H.\text{Adv}$). Eq. (3) was simplified to the following conservation equation for mixed-layer DIC:

$$\frac{dDIC}{dt} = \frac{F}{h} + \frac{1}{h} \Theta \left(\frac{dh}{dt} \right) (DIC_{tc} - DIC) + J_{trsp} - J_{ncp} + \psi, \quad (4)$$

where the last term on the right-hand side, ψ , is the model error.

Eq. (4) was applied by means of a vertically one-dimensional box representation of the mixed-layer. This is shown schematically in Fig. 8. The upper box represents the mixed-layer, and the lower box the thermocline. The mixed-layer box exchanges CO₂ with the atmosphere across the air-sea interface. The boundary between the mixed-layer and the thermocline is permitted to move up and down depending on the (monthly mean) mixed-layer depth (Fig. 9). The

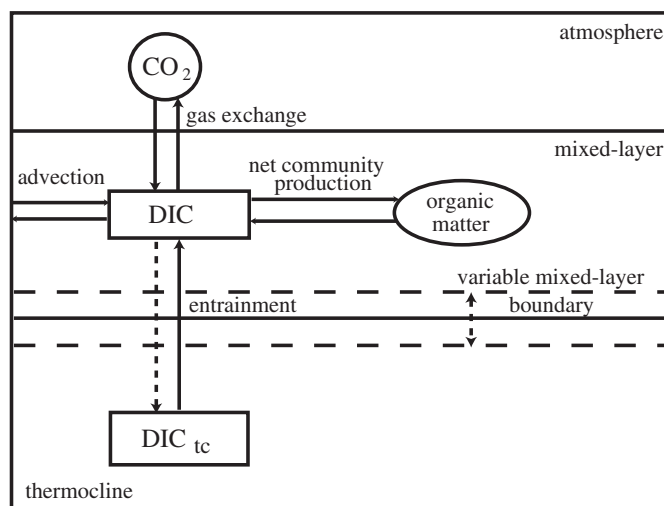


Fig. 8. (a) Schematic representation of the one-dimensional, two box, ocean model used in the study of the seasonal carbon cycle on the Scotian Shelf. Dissolved inorganic carbon is modeled only in the mixed-layer. The other carbon reservoirs are only included to establish boundary conditions. The depth of the mixed-layer is variable, thereby entraining carbon-rich water from the thermocline (tc). Figure modified from Gruber et al. (1998).

concentration of DIC was assumed homogeneous in the mixed-layer. Horizontal transport (J_{trsp}) moves water through the mixed-layer. The relationship between salinity normalized TA ($TA_{norm} = 35TA/S$) and salinity revealed nearly conservative behaviour (Fig. 6 inset), which could support an assumption that calcification can be neglected, despite evidence of summer coccolithophore blooms in the region (Brown and Yoder, 1993; Townsend et al., 1994). There appears to be an accumulation of TA near $S = 35$, present in both the observed and normalized TA, which may indicate the dissolution of CaCO₃. However, waters of $S = 35$ are representative of samples collected in the deeper water column, significantly further offshore than station HL2 (Fig. 1). Furthermore, with discrete TA samples from only seasonal cruises, the coarse temporal resolution prevents the confirmation or exclusion of calcification in the region (see Section 4.2 for further discussion of this matter). The possible contribution from sedimentary processes was neglected. It was also assumed that the surface mixed-layer is isolated from the sea-floor; the water depth at HL2 is roughly 200 m, and the depth of the mixed-layer ranged from 10 to 60 m at the annual scale (Fig. 9).

3.2.1. Model inputs

The diagnostic model analysis of the seasonal carbon cycle in the mixed-layer was restricted to the year 2008, when measurements are available at the monthly timescale. The depth of the mixed-layer was estimated from profiles of temperature from monthly occupations at the mooring site (Fig. 9). The thickness of the surface mixed-layer shows a large seasonal variability, mainly caused by changes in

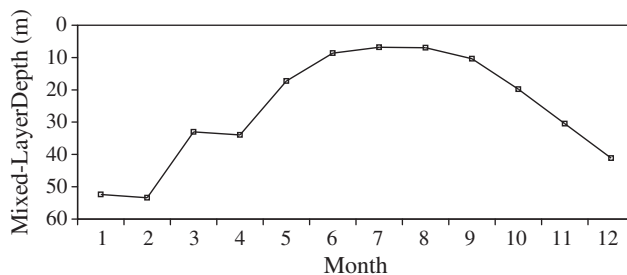


Fig. 9. Monthly values of mixed-layer depth estimated from profiles of temperature at station HL2.

surface wind-stress and heat exchange. Monthly values of ($dDIC/dt$) were computed (i.e. $dDIC/dt$ in February was computed from: $DIC_{Feb} - DIC_{Jan}$) from the annual time series of mixed-layer DIC (Fig. 7a).

Monthly values of air–sea CO_2 flux were computed according to the method described in Section 3.1. The transport term, which also includes the contributions from horizontal and vertical diffusion, and horizontal and vertical advection, was estimated empirically using the relationship between DIC and salinity. Discrete DIC samples are plotted against the corresponding measured salinity ($n = 784$, $r^2 = 0.74$, $p < 0.001$, standard error = $22 \mu mol kg^{-1}$) in Fig. 10. Please note that these discrete data are independent of the annual cycle of DIC and salinity obtained from the CARIOCA buoy. The salinity-dependent changes in DIC, which were assumed to be due to horizontal transport, and vertical and horizontal diffusion, are described by this relationship,

$$DIC_S = 46.5S + 546.4, \quad (5)$$

and

$$J_{trsp} = \frac{dDIC_S}{dt}. \quad (6)$$

We assumed that local salinity-dependent processes such as precipitation and evaporation could be neglected. Previous studies have used the seasonal differences in the relationship between DIC and salinity to evaluate the salinity-dependent changes in DIC (Thomas and Schneider, 1999; Osterroht and Thomas, 2000; Bozec

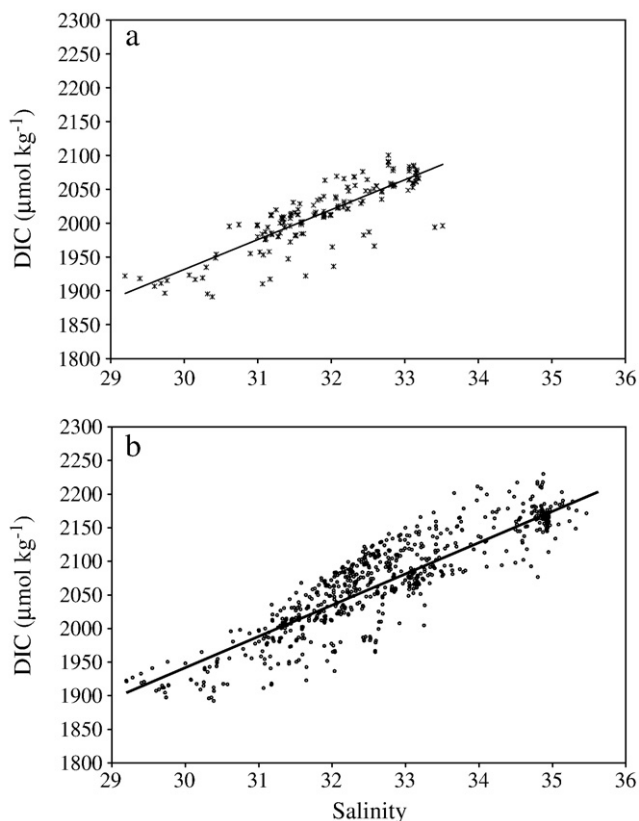


Fig. 10. DIC and salinity data obtained from discrete samples collected throughout the Scotian Shelf at all stations shown in Fig. 1 on spring and autumn cruises. (a) DIC samples from the surface mixed-layer and a linear regression for these data ($DIC_S = 44.4s + 601$, $n = 181$, $r^2 = 0.71$, $p < 0.001$). This relationship was used to compute the salinity-dependent changes in DIC to approximate the J_{trsp} term (Eqs. (5) and (6)). (b) DIC samples from the subsurface layer and a linear regression for these data ($DIC_S = 46.5S + 546$) ($n = 784$, $r^2 = 0.74$, $p < 0.001$).

et al., 2006). This method of empirically isolating changes due to horizontal transport does not allow for a complete description of the horizontal processes in the region. However, its inclusion in the 1-D approach presented here, allowed changes due to transport and biology, often grouped together (Olsen et al., 2008; Omar et al., 2010), to be unraveled.

The vertical entrainment term was quantified based on DIC concentration below the mixed layer. DIC_{tc} was taken from measured profiles of DIC from the mooring site (Fig. 13a). For the months when a measured profile of DIC was not available (Feb, Jul, Nov, and Dec) Eq. (4) was used to compute a profile of DIC from the observed profile of salinity at HL2 for that month, and from this an estimate of DIC_{tc} was made.

The change in DIC due to biology (J_{ncp}) was then computed from the DIC conservation equation:

$$-J_{ncp} = \frac{dDIC}{dt} - \frac{F}{h} - \frac{1}{h} \Theta \left(\frac{dh}{dt} \right) (DIC_{tc} - DIC) - \left(\frac{dDIC_S}{dt} \right) - \psi, \quad (7)$$

where the last two terms on the right-hand side are J_{trsp} estimated using Eq. (6), and ψ , which represents the error.

3.2.2. Error estimation

The uncertainty in the computed J_{ncp} term includes the uncertainty associated with each of the terms in Eq. (7). The pCO_2 measurements were accurate ($2 \mu atm$), and the error associated with the DIC computation (from known values of pCO_2 and TA) is fairly small (less than $10 \mu mol kg^{-1}$) (Dickson, 1990). However, we computed DIC from the hourly time series of pCO_2 and the hourly estimate of TA, based on the relationship between TA and S (Fig. 6) and the hourly salinity data from the CARIOCA buoy (Fig. 5). The standard error associated with the computation of TA from salinity was $12 \mu mol kg^{-1}$, which we considered as a reasonable estimate of the uncertainty associated with computed time series of DIC. The monthly change in DIC ($dDIC/dt$) had an associated uncertainty ranging from 0.1 to $0.7 mol C m^{-2} month^{-1}$. There is a relatively large error associated with the air–sea CO_2 flux term, resulting from the parameterization of the gas transfer velocity (Watson et al., 2009). We computed the air–sea CO_2 flux using the parameterization of Wanninkhof (1992). The uncertainty associated with the monthly air–sea flux was determined from the mean difference between the flux computed with the parameterization of Wanninkhof (1992) and the flux computed with the parameterization of Nightingale et al. (2000). The uncertainty associated with the air–sea CO_2 flux ranged from 0.01 to $0.2 mol C m^{-2} month^{-1}$. The vertical gradients used to compute the vertical entrainment term were small compared to the measured values and had the same uncertainty as the discrete DIC measurements (on the order of $5 \mu mol kg^{-1}$). The uncertainty associated with the monthly estimates of the vertical entrainment term ranged from 0.04 to $0.3 mol C m^{-2} month^{-1}$. The relationship between DIC and salinity (Fig. 10) indicated that 74% of the variability in DIC is due to changes in salinity. The uncertainty in the J_{trsp} term was therefore assumed to be equal to 26% of the observed monthly change in mixed-layer DIC, and ranged from 0.03 to $0.53 mol C m^{-2} month^{-1}$. The uncertainty in each of the terms on the right-hand side of Eq. (6) was propagated to estimate the uncertainty associated with J_{ncp} which ranged from 0.12 to $0.77 mol C m^{-2} month^{-1}$.

The model uncertainty (ψ) was estimated by means of a Monte Carlo simulation of J_{ncp} (with the simulated series referred to as J_{ncp}^*), and it was assumed that a reasonable estimate of ψ was the standard deviation of J_{ncp}^* . The inputs for the simulation were randomly generated from distributions which most closely match the data; 10,000 points were chosen randomly for each of the model variables using random number generators in MATLAB (Mathworks, Inc.). Following a test for normality and uniformity, a normal distribution was used for the ' $dDIC/dt$ ' and ' J_{trsp} ' (or $dDIC_S/dt$) terms, and a uniform distribution was used for the

'vertical entrainment' and 'flux' terms. The uniform distribution requires the maximum value, while the normal distribution requires the mean and standard deviation. These values were taken from the monthly values of each of the terms on the right hand side of Eq. (7):

$$J_{ncp}^* = M_{dDIC/dt} - M_{Flux} - M_{V,Ent} - M_{Jtrsp}, \quad (8)$$

where 'M' indicates the randomly generated series. The equation was solved for J_{ncp}^* (10,000 times), and the standard deviation of J_{ncp}^* used as the magnitude of ψ . The resulting uncertainty is $15 \mu\text{mol kg}^{-1}$, or 0.5 mol C m^{-2} using an annual average mixed-layer depth of 27 m. The uncertainty estimated with the Monte Carlo approach was roughly equal to the mean of the uncertainty estimated with the conventional error propagation.

4. Results

4.1. The annual cycle of $p\text{CO}_2$

The partial pressure of CO_2 in seawater is controlled by several physical and biogeochemical factors. Changes in temperature, salinity, alkalinity, and DIC will influence $p\text{CO}_2$, with changes in temperature and DIC having the strongest influence. Hourly measurements of surface

water $p\text{CO}_2$ from January to December are given in Fig. 4b. Wintertime $p\text{CO}_2$ indicated supersaturation with respect to the atmosphere and had a relatively constant value of roughly $420 \mu\text{atm}$. The onset of the spring phytoplankton bloom can clearly be seen in early April with a sharp drop in $p\text{CO}_2$ to a minimum value of roughly $240 \mu\text{atm}$ over a period of less than two weeks. The post-bloom recovery was seen over the next 120 days, coincident with the summer warming of the surface waters from yearday 100 to yearday 225 (Fig. 5). The $p\text{CO}_2$ quickly reached supersaturation, with a maximum $p\text{CO}_2$ of roughly $460 \mu\text{atm}$ at yearday 225. At roughly yearday 225 there was a short-term increase in $p\text{CO}_2$ which was immediately followed by a decrease in $p\text{CO}_2$ of roughly $50 \mu\text{atm}$. The increase in $p\text{CO}_2$ was coincident with an increase in DIC and salinity and a decrease in temperature and is possibly the result of vertical mixing. After yearday 230 a period of fairly constant $p\text{CO}_2$ extends from early September to the end of the year. The autumn bloom, though evident in satellite images of the region, was not visible in the $p\text{CO}_2$ time series. While this second bloom is smaller than the spring bloom (Greenan et al., 2004), it occurs as surface waters are cooling, which should act to enhance the decrease in $p\text{CO}_2$. Despite the combined effect of photosynthesis and decreasing water temperature, the autumn bloom, as a single, short-term event, remained undetected within the higher frequency variability of the $p\text{CO}_2$ observations.

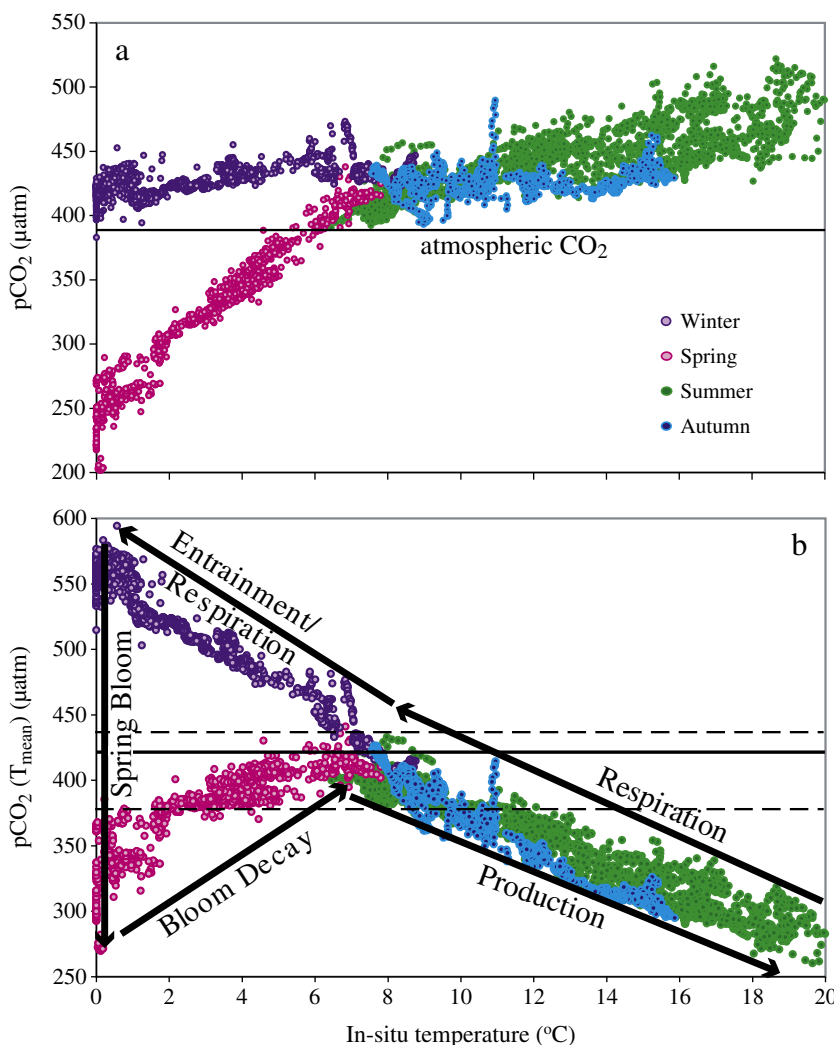


Fig. 11. All values of $p\text{CO}_2$ are normalized to a constant, annual mean temperature of $T_{\text{mean}} = 7.0 \text{ }^\circ\text{C}$, and plotted versus their observed temperature. The average value of $p\text{CO}_2(T_{\text{mean}})$ at T_{mean} is given by the solid line ($415 \mu\text{atm}$), while the maximum (435) and minimum (375) values at this temperature are given by the dashed lines. The dominant mechanisms acting in each of the seasons are shown schematically by the black arrows. The spring values (pink) include the months April and May; the summer values (green) include June, July, and August; the autumn values (blue) include September and October; and the winter values (purple) include last week of December, January, February and March.

Calcification during the autumn bloom would increase the $p\text{CO}_2$, potentially masking the drawdown by photosynthesis. However, we cannot presently confirm, or exclude the contribution from calcification.

Hourly $p\text{CO}_2$ data during the 2008 spring phytoplankton bloom are shown in Fig. 4a. The bloom was initiated on April 6th, and lasted roughly 8 days, until the 14th of April, when $p\text{CO}_2$ concentrations began to increase. The $p\text{CO}_2$ and DIC concentrations at the onset of the bloom were $424 \mu\text{atm}$ and $2070 \mu\text{mol kg}^{-1}$ respectively. The $p\text{CO}_2$ and DIC concentration at the termination of the bloom were $294 \mu\text{atm}$ and $1987 \mu\text{mol kg}^{-1}$ respectively. The depth of the mixed layer at the mooring station was 30 m, measured on an April 10th occupation of station HL2. The resulting carbon draw-down over the bloom period was $\Delta\text{DIC}_{\text{bio}} = 1.7 \text{ mol C m}^{-2}$. Assuming no other source or sink was acting during this period, this drawdown was ascribed to biological uptake.

In-situ $p\text{CO}_2$ is plotted against in-situ SST, with the seasons distinguished by color in Fig. 11a. The large range in surface temperature, particularly in the transition from spring to summer, and summer to autumn, from near zero to roughly 20° can be seen. There is a correspondingly large range in $p\text{CO}_2$ from roughly $200 \mu\text{atm}$ at the height of the spring bloom (Fig. 11a, in pink), to greater than $500 \mu\text{atm}$ at the maximum SST (Fig. 11a, in green). By contrast, the autumn (Fig. 11a, in blue) and winter (Fig. 11a, in purple) $p\text{CO}_2$ are roughly constant between $400 \mu\text{atm}$ and $450 \mu\text{atm}$, indicating supersaturation with respect to atmospheric CO_2 over this period. The effect of temperature on $p\text{CO}_2$ is well understood from thermodynamic relationships, allowing the correction of the observed time series, $p\text{CO}_2(\text{obs})$, to a mean temperature, T_{mean} , via the equation of Takahashi et al. (2002):

$$p\text{CO}_2(T_{\text{mean}}) = p\text{CO}_2(\text{obs})[\exp(0.0423(T_{\text{mean}} - T_{\text{obs}}))]. \quad (9)$$

Values of $p\text{CO}_2$ corrected to a constant, annual mean, temperature ($T_{\text{mean}} = 7.0^\circ\text{C}$) are plotted against in-situ temperature (T_{obs}) in Fig. 11. The spring values (in pink) show the April $p\text{CO}_2$ minimum due to phytoplankton bloom, and the post-bloom recovery when DIC was resupplied due to respiration and remineralization. The decay of the bloom was coincident with the onset of surface warming. The summertime values (in green) ranged from 6°C to 20°C ; $p\text{CO}_2$ was reduced due to on-going photosynthesis and to out-gassing driven by the warming of the waters. The post-bloom, summer, production is discussed in more detail in Section 5.1. In autumn $p\text{CO}_2$ was reduced and increased steadily as the water cooled, reflecting the transition between production and respiration in the system. In contrast to the other seasons, the winter values (in purple) covered a much smaller range in water temperature, which was fairly constant during this period. The winter data showed increased values of $p\text{CO}_2$ due to respiration and entrainment of carbon-rich subsurface waters. Factors other than temperature were investigated in detail by looking at the variability of surface DIC concentration over the annual cycle.

4.2. The annual cycle of DIC

As described by Eq. (3), DIC is affected by the air–sea flux of CO_2 , vertical diffusion and entrainment, horizontal advection, and biological production. The annual cycle of mixed-layer DIC is shown in Fig. 7a. The normalization of DIC (and TA) to a constant salinity removes the effect of freshwater fluxes from the measured concentrations. Variability in the salinity normalized concentrations (DIC_{norm} and TA_{norm} , Fig. 7b) is thus primarily controlled by water temperature (i.e., by the solubility of CO_2), biological processes, air–sea exchange of CO_2 , and the mixing of water masses. The DIC drawdown by the spring phytoplankton bloom was visible in both the observed and normalized DIC (Fig. 7). However, the continued decrease in DIC seen after yearday 150 is significantly reduced in the time series of DIC_{norm} , indicating the dominance of advection (J_{trsp}) over this period.

Similarly, the late summer decrease in TA was absent from the time series of TA_{norm} , and there was a modest increase in TA over the period from roughly yeardays 175 to 275, as a result of the arrival of St. Lawrence River water, which has a non-zero TA at $S=0$, and highlights the limitation of the salinity-normalization for river-influenced waters (Friis et al., 2003). Between yeardays 200 and 250, there was a significant increase in DIC (Fig. 7). This could indicate dissolution of CaCO_3 which would add DIC, and TA, to the system, decreasing the $p\text{CO}_2$. However, over the same period, there was an increase in salinity, and a decrease in temperature (Fig. 5), along with an increase in $p\text{CO}_2$ (Fig. 4b). An alternate explanation is that increase in DIC (salinity and $p\text{CO}_2$) was the result of the upward mixing of DIC-rich water from below, confirmed by the decrease in temperature over the same period. However, since the annual cycle of DIC was computed from measurements of $p\text{CO}_2$ and computed values of TA, based on a relationship between TA and salinity, we cannot exclude or confirm any contribution from the formation/dissolution of CaCO_3 which would require direct measurements of TA (or an additional parameter of the CO_2 system) with the same temporal resolution as the $p\text{CO}_2$ time-series.

The flux of CO_2 between the ocean and the atmosphere either adds (by invasion), or removes (by out-gassing), DIC from the surface waters. The annual cycle of air–sea CO_2 flux is shown in Fig. 12. The surface waters on the Scotian Shelf acted as a net source of CO_2 to the atmosphere for most of the year, with a reversal of this process occurring only for a short period during, and following, the spring phytoplankton bloom. There was therefore a reduction in the surface water DIC pool as a result of out-gassing; the annual air–sea flux was $F = -1.4 \text{ mol C m}^{-2} \text{ yr}^{-1}$.

Profiles of DIC from April (spring), August (summer), and October (autumn) occupations at station HL2 are shown in Fig. 13a. The corresponding profiles of apparent oxygen utilization ($\text{AOU} = [\text{O}_2]_{\text{sat}} - [\text{O}_2]_{\text{obs}}$), are shown in Fig. 13b. The oxygen profiles are from same (monthly) occupations of station HL2 as the temperature and salinity profiles. Dissolved oxygen ($[\text{O}_2]_{\text{obs}}$) was measured using a Sea-Bird electrochemical oxygen sensor. The saturation oxygen concentration was computed for the observed

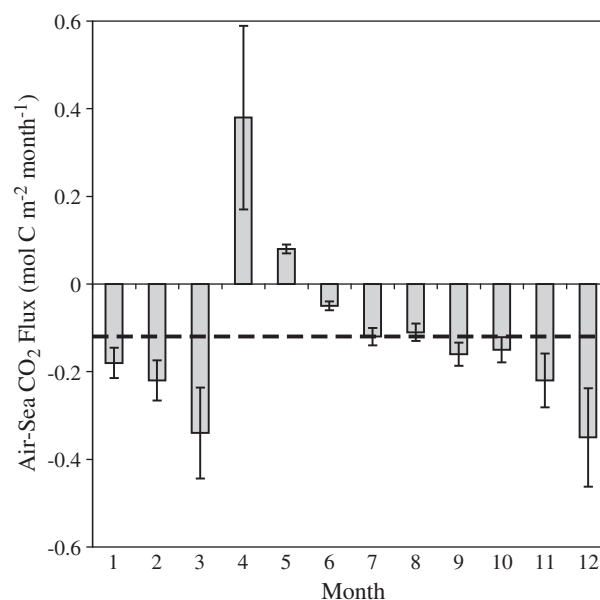


Fig. 12. Annual cycle of air–sea CO_2 fluxes computed using $p\text{CO}_2$ data from the CARIOCA buoy. The uncertainty is estimated from the difference between monthly fluxes computed using the wind speed parameterization of Wanninkhof (1992) and Nightingale et al. (2000). Annual integration of these monthly fluxes yields an out-gassing of $-1.4 \text{ mol C m}^{-2} \text{ yr}^{-1}$ (see also Table 2). The corresponding annual monthly flux ($F_{\text{mean}} = -0.12 \text{ mol C m}^{-2} \text{ month}^{-1}$) is indicated by the black dashed line.

temperature, salinity and pressure. It can be seen that with the onset of the spring bloom, which occurs at the temperature minimum, the surface waters quickly became undersaturated with respect to CO₂. DIC in the surface waters was reduced due to photosynthesis, while negative surface values of AOU corresponded to a production of oxygen by the phytoplankton. Organic matter was exported to the subsurface layer, and remineralization of this organic matter increased the concentration of DIC in waters below a depth of roughly 40 m. The positive subsurface AOU concentrations reflect this remineralization, or respiration, process. Primary production was reduced, though ongoing, in summer and autumn, when surface DIC concentrations were additionally influenced by the input of freshwater from the outflow of the Gulf of St. Lawrence. The ongoing biological production in summer and autumn was confirmed by the negative values of surface AOU in both August and October. Respiration further increased DIC, and AOU, in the subsurface layer in summer and autumn, while the deepening of the mixed-layer in winter introduced DIC-rich waters from below the thermocline into the surface layer.

4.3. Model results

The monthly changes in DIC due to vertical entrainment, lateral transport (Jtrsp), air–sea flux, biological production (Jncp), and the total observed monthly changes are shown in Figs. 14 and 15a. The air–sea flux makes a negative contribution to changes in DIC and as described above, the region acted as a source of CO₂ to the atmosphere over the annual scale. Vertical entrainment delivered DIC-rich waters to the mixed-layer from June to November (Fig. 14e). The impact of transport was greatest in the second half of the year, both increasing and decreasing mixed-layer DIC concentration (Fig. 14d). The change in DIC due to biology dominated the total change in spring, with a diminishing influence over the rest of the year. There was a persistent biological signal throughout the year on the Scotian Shelf (Fig. 14e), despite the apparent depletion of nutrients following the spring phytoplankton bloom. Respiration increased DIC from November to March and in May due to the decay of the spring bloom. Production of organic matter occurred in April and from June to October. The most important processes for variability of DIC in the surface mixed-layer

were biological production, and to a lesser extent, entrainment, and transport (Fig. 15).

The changes in pCO₂ due to temperature, vertical entrainment, Jtrsp and Jncp are illustrated in Fig. 15b. The temperature control was computed with the initial value of pCO₂ (in January) and subsequent monthly values computed by assuming that the only change was that of temperature. For example, the water cooled by 1.5 °C between January and February, which corresponds to a 6% decrease in pCO₂ (from roughly 420 μatm in January to roughly 395 μatm in February) applying the empirical relationship between temperature and pCO₂ of Takahashi et al. (2002) assuming no process other than temperature was acting on the pCO₂. Between February and April, the water temperature remained constant; the increase in temperature from April (0.8 °C) to August (17 °C) corresponded to an increase in pCO₂ of nearly 70% (Fig. 15b); the estimated uncertainty associated with (monthly values of) this term was 10 μatm. The effect of vertical entrainment, Jtrsp and Jncp on pCO₂ was computed via the following method. The initial pCO₂ was computed as a function of the initial (empirically derived) DIC and TA:

$$pCO_2^{t=0} = f(DIC_0, TA_0), \quad (10)$$

where the subscripts on DIC and TA refer to these initial values. The change in pCO₂ to Jtrsp (pCO₂(Jtrsp)) was then computed from the initial value of pCO₂, the initial value of DIC, the change in DIC due to Jtrsp in the month of January, and the January TA concentration, with the following equation:

$$pCO_2^{t=1}(Jtrsp) = f(DIC_0 + DIC_{Jtrsp1}, TA_1), \quad (11)$$

where DIC_{Jtrsp1} is the change in DIC due to Jtrsp in January (see Table 2). The same procedure was followed for each month, for vertical entrainment, and for Jncp (Fig. 15b). The uncertainty associated with monthly values of pCO₂(Jtrsp), pCO₂(Vent), and pCO₂(Jncp) was estimated to be 40 μatm.

The large seasonal amplitude of surface water temperature is particularly important to the carbon system on the Scotian Shelf. The region experiences near, or sub-zero temperatures during the winter season, due to its position downstream of the Labrador Sea and the

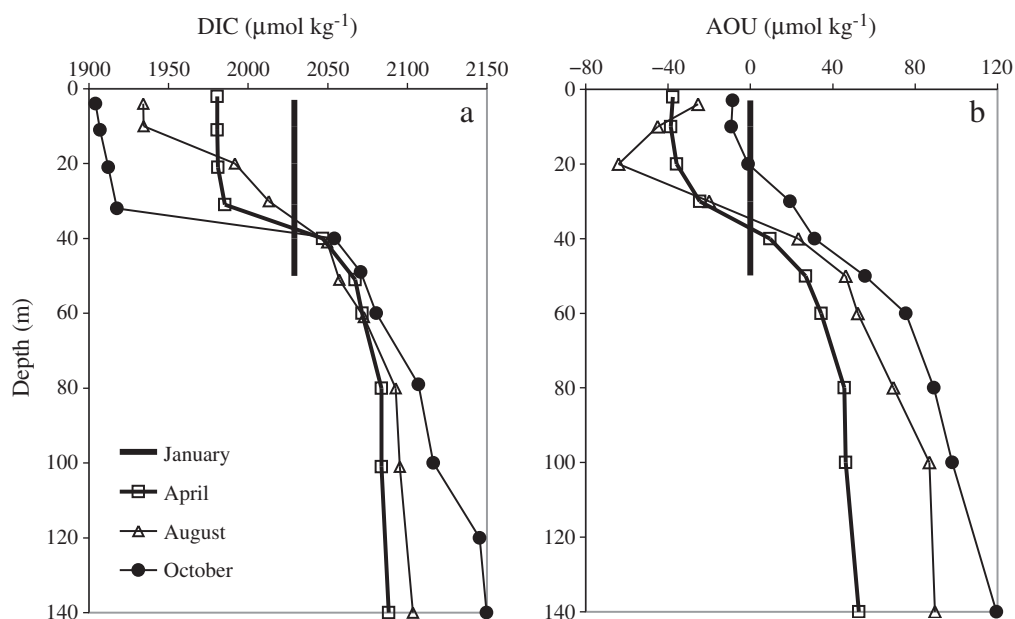


Fig. 13. Profiles of (a) DIC and (b) AOU in January, April, August, and October. The April, August, and October profiles result from discrete measurements of samples collected at the mooring site. The January DIC profile was estimated from the January surface DIC concentration, and the corresponding mixed-layer depth. The January AOU profile was estimated from the saturation oxygen concentration using the January values of surface salinity and temperature, and mixed-layer depth.

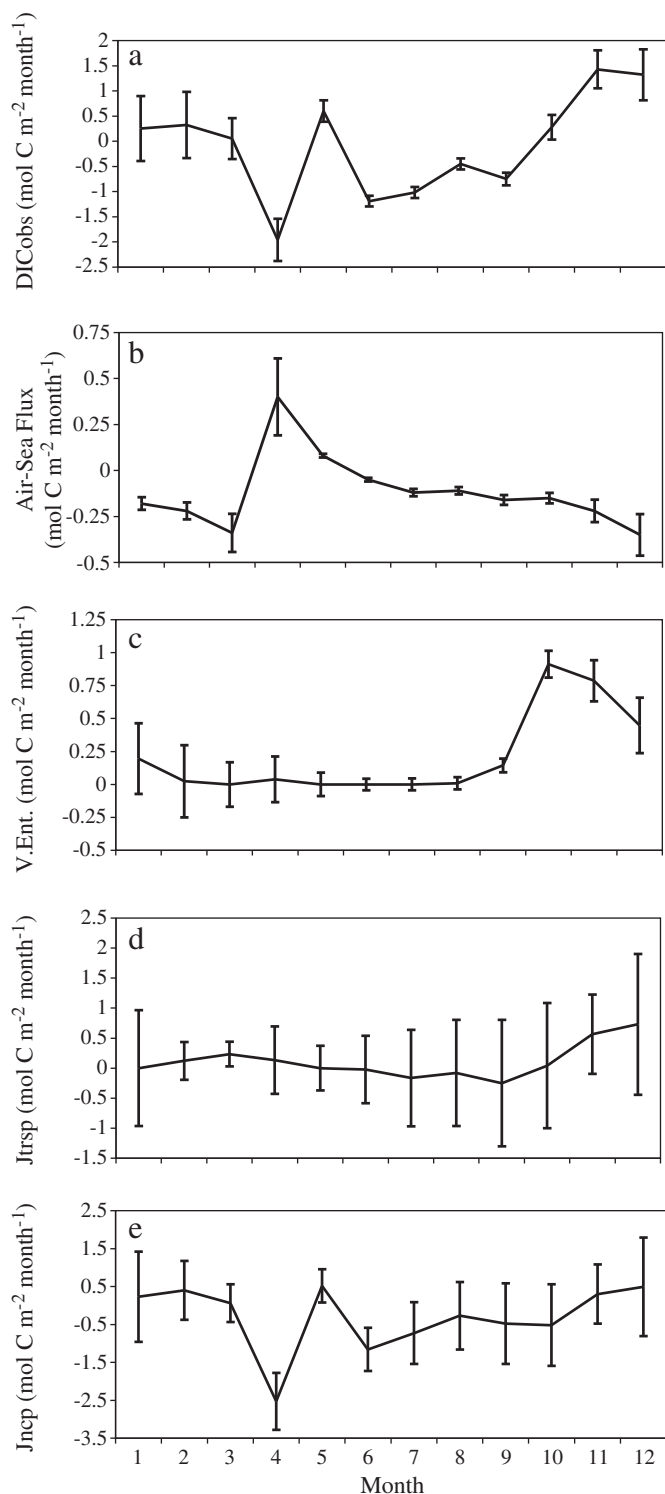


Fig. 14. The annual cycles of each of the terms in Eq. (6): (a) the observed monthly change ($dDIC/dt$), (b) the air–sea CO_2 flux, (c) vertical entrainment, (d) J_{trsp} , and (e) J_{ncp} .

Gulf of St. Lawrence. Temperatures peak at nearly $20\text{ }^\circ\text{C}$ in the late summer due to the region's latitude and the relatively stable, stratified water column throughout the summer season. As discussed in more detail in Section 5.1, this large amount of surface warming was only partially off-set by biological production, and surface waters however remained supersaturated throughout the year, outside of the brief spring bloom period. Biological production was reduced in autumn, while over the same period the waters cooled, and the winds strengthened introducing DIC-rich waters from below and resulting

in the continued supersaturation with respect to the atmosphere. The absence of biology from June to September would result in a near doubling of surface pCO_2 compared to the observed in-situ values (Fig. 15b). The region acted a source of CO_2 to the atmosphere despite the productivity of the shelf, due to the magnitude of the temperature control. The waters at station HL2 originate in the cold, biologically productive Gulf of St. Lawrence, as these waters move south via the Nova Scotia current they warm, increasing the surface pCO_2 . The Scotian Shelf is also subject to episodic upwelling, and wind and convective mixing all of which contribute to the autumn and winter destratification of the water column enhancing the surface water pCO_2 . Schiettecatte et al. (2006) found that the Scheldt plume in Belgian coastal waters of similar latitude is similarly supersaturated outside of the spring bloom period, but concluded that the biological control in this system dominated the temperature control. These results highlight the importance of case-by-case studies of the carbon system in coastal ocean environments.

4.4. Net community production

Net community production (NCP) is the difference between net primary production (NPP) and heterotrophic respiration (R):

$$NCP = NPP - R. \quad (12)$$

Quantifying changes in DIC due to photosynthesis and respiration, i.e. (J_{ncp}), allowed the annual NCP ($2.4\text{ mol C m}^{-2}\text{ yr}^{-1} = 29\text{ g C m}^{-2}\text{ yr}^{-1}$, computed as the sum of the monthly values of J_{ncp} with the opposite sign, such that production represents positive NCP, but a loss of DIC, or negative J_{ncp}) to be estimated (see Table 2). A satellite-based estimate of annual primary production (PP) based on particulate organic carbon (POC) was made using the Giovanni online data system (Acker and Leptoukh, 2007). The annual PP on the Scotian Shelf resulting from the POC estimate was $PP_{SAT} = 95\text{ g C m}^{-2}\text{ yr}^{-1}$, which is in general agreement with the literature values which range from 60 to $130\text{ g C m}^{-2}\text{ yr}^{-1}$ (Mills and Fournier, 1979; Mousseau et al., 1996). Our estimate of annual NCP ($2.4\text{ mol C m}^{-2}\text{ yr}^{-1}$ or $28\text{ g C m}^{-2}\text{ yr}^{-1}$) thus corresponded to approximately 30% of PP (using an average value of $PP = 95\text{ g C m}^{-2}\text{ yr}^{-1}$).

An additional, independent, estimate of NCP can be made by exploiting the time-series of chl-a measured by the CARIOCA buoy. Biomass (B) was estimated from the time-series of chl-a and carbon-to-chlorophyll ratio $70\text{ mg C (mg Chl)}^{-1}$ (Fig. 16). While not accounting for a possible seasonal variability in the carbon-to-chlorophyll ratio, this value is consistent with literature values for the Scotian Shelf region (Platt et al., 1991). The biomass based estimate of NCP ($NCP_B = 1.5\text{ mol C m}^{-2}\text{ yr}^{-1} = 18\text{ g C m}^{-2}\text{ yr}^{-1}$) was computed from the annual integral of monthly biomass estimates. The uncertainty (70%) reflects the uncertainty in the chlorophyll-to-carbon ratio estimate. Compared to the above DIC-based assessment, the biomass based estimate appeared to underestimate NCP. This underestimate may be due to the substantial losses of chl-a from the surface layer due to sinking and grazing (up to 45% of the surface waters being cleared of particles in a given day, e.g. Banse, 1994; Banse, 1995). These losses diminish the chl-a concentration, thus leading to lower observed values, although DIC has been consumed. In other words, while the above DIC based NCP estimate includes this carbon uptake, the chl-a based estimate (NCP_B) does not and would produce lower chl-a values which would result in an underestimate of carbon uptake. Furthermore, the chl-a signal (Fig. 16) was driven primarily by the spring bloom, while in late spring and summer, only modest chl-a concentrations were observed. However, we provide evidence here (see also Section 5.1) of substantial carbon uptake in the late spring and summer, after the exhaustion of nutrients (see for example Fogg, 1983; Thomas et al., 1999, and Schartau et al., 2007), which cannot be accounted for by the

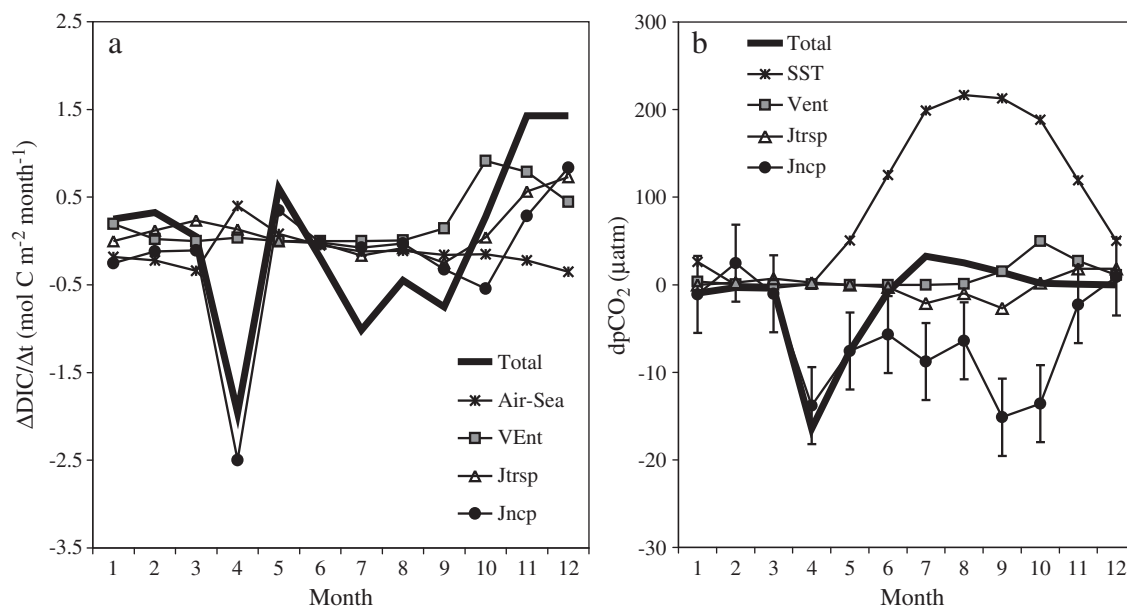


Fig. 15. (a) Computed monthly variations of DIC in units of $\text{mol C m}^{-2} \text{ month}^{-1}$. The total change ($d\text{DIC}/dt$), the change due to air–sea exchange of CO_2 , vertical entrainment, transport (Jtrsp), and net community production (Jncp) are shown. (b) The controls on $p\text{CO}_2$, shown as cumulative values relative to January.

chl-a based NCP_B estimated. As discussed in detail by Shadwick et al. (2010), this discrepancy has serious implications for satellite based assessments of NCP, or related CO_2 fluxes (e.g. Lefèvre et al., 2002; Chierici et al., 2009), since even modest carbon uptake in summer may strongly influence surface water $p\text{CO}_2$ due to the shallow summer mixed-layer. Inorganic carbon based approaches, such as the investigation presented here, may therefore play an essential role in constraining optical, space-borne, or in-situ approaches.

5. Discussion

5.1. Post-bloom summer production

Production in the Scotian Shelf region was ongoing after the decay of the spring phytoplankton bloom and the exhaustion of surface nutrients as evidenced by in-situ observations of DIC and AOU in summer and autumn (Fig. 13), and by the model estimate of Jncp (Table 2). The uptake of more DIC than expected from the canonical Redfield ratios is often referred to as carbon overconsumption (Redfield et al., 1963; Toggweiler, 1993). This non-Redfield produc-

tion or carbon overconsumption has been widely observed and discussed (Droop, 1973; Sambrotto et al., 1993; Thomas et al., 1999; Osterroht and Thomas, 2000; Arrigo, 2005; Schartau et al., 2007). New production, as defined by Dugdale and Goering (1967) is the production by phytoplankton based on the conversion from nitrate uptake to carbon uptake using the elemental (Redfield) ratio found in organic matter. During the month of April we assume that the NCP was equal to net primary production in the region, which is compared to new production. We estimated new production on the Scotian Shelf from the difference in surface nitrate concentrations between the end of March ($6.23 \mu\text{mol kg}^{-1}$) and the end of April ($0.28 \mu\text{mol kg}^{-1}$), after the spring bloom. The total change in nitrate was $\Delta\text{NO}_3 = 5.95 \mu\text{mol kg}^{-1}$, which corresponds to an inorganic carbon uptake of $\Delta\text{DIC}_N = 39.42 \mu\text{mol kg}^{-1} = 1.3 \text{ mol C m}^{-2}$, using the Redfield ratio of C:N = 106:16, and a mixed-layer depth of 34 m (see Table 2). If this is compared to the computed biological DIC draw-down in April ($\Delta\text{DIC}_{\text{bio}} = 2.4 \text{ mol C m}^{-2}$ and Table 2), new production accounted for roughly 54% of the DIC drawdown observed during the spring bloom. Please note that this simplified approach of comparing NO_3 concentration from one month to the next does not account for the several

Table 2
The monthly estimates of each of the terms used in the computation of Jncp (see Eq. (6)). The monthly mean DIC concentration and the monthly estimates of $\text{DIC}_{\text{ic}} - \text{DIC}$ are given in $\mu\text{mol kg}^{-1}$ (columns 2 and 3). In the fourth column, the monthly change in DIC, $d\text{DIC}/dt$ is given in $\mu\text{mol kg}^{-1} \text{ month}^{-1}$, and in the fifth column, the monthly change (dC/dt) is given in units of $\text{mol C m}^{-2} \text{ month}^{-1}$. The air–sea CO_2 flux (F_{CO_2}), vertical entrainment (V.Ent), Jtrsp and Jncp are given in $\text{mol C m}^{-2} \text{ month}^{-1}$. The (net) annual contributions to changes in DIC are given in the last row in units of $\text{mol C m}^{-2} \text{ yr}^{-1}$.

Month	DIC	$\text{DIC}_{\text{ic}} - \text{DIC}$	$d\text{DIC}/dt$	dC/dt	F_{CO_2}	h	dh/dt	V.Ent.	Jtrsp	–Jncp
1	2058	37	2	0.12 ± 0.64	-0.18 ± 0.03	52	11	0.43 ± 0.27	0.00 ± 0.03	-0.14 ± 0.70
2	2060	24	3	0.14 ± 0.66	-0.22 ± 0.05	53	1	0.02 ± 0.27	0.12 ± 0.03	0.22 ± 0.71
3	2066	13	6	0.19 ± 0.41	-0.34 ± 0.10	33	–20	0.00 ± 0.17	0.23 ± 0.05	0.30 ± 0.45
4	2006	29	–60	-2.08 ± 0.42	0.40 ± 0.21	34	1	0.03 ± 0.17	0.13 ± 0.50	-2.64 ± 0.71
5	2021	14	15	0.26 ± 0.21	0.08 ± 0.01	17	–17	0.00 ± 0.09	0.00 ± 0.06	0.18 ± 0.24
6	2019	21	–2	-0.01 ± 0.11	-0.05 ± 0.01	9	–8	0.00 ± 0.04	-0.02 ± 0.00	0.06 ± 0.12
7	1986	48	–33	-0.30 ± 0.11	-0.12 ± 0.02	9	0	0.00 ± 0.05	-0.06 ± 0.07	-0.12 ± 0.14
8	1962	89	–24	-0.23 ± 0.11	-0.11 ± 0.02	9	0	0.09 ± 0.05	-0.07 ± 0.05	-0.14 ± 0.13
9	1948	130	–14	-0.15 ± 0.13	-0.16 ± 0.03	10	1	0.18 ± 0.05	-0.14 ± 0.04	-0.03 ± 0.15
10	1957	115	9	0.19 ± 0.24	-0.15 ± 0.03	20	10	1.12 ± 0.10	-0.04 ± 0.04	-0.75 ± 0.27
11	2003	72	46	1.45 ± 0.37	-0.22 ± 0.06	31	11	0.79 ± 0.16	0.56 ± 0.35	0.32 ± 0.54
12	2056	65	52	2.22 ± 0.51	-0.35 ± 0.11	41	11	0.71 ± 0.21	1.46 ± 0.53	0.39 ± 0.77
Annual			0	1.80 ± 1.31	-1.42 ± 0.28			3.38 ± 0.55	2.20 ± 0.82	-2.36 ± 2.21

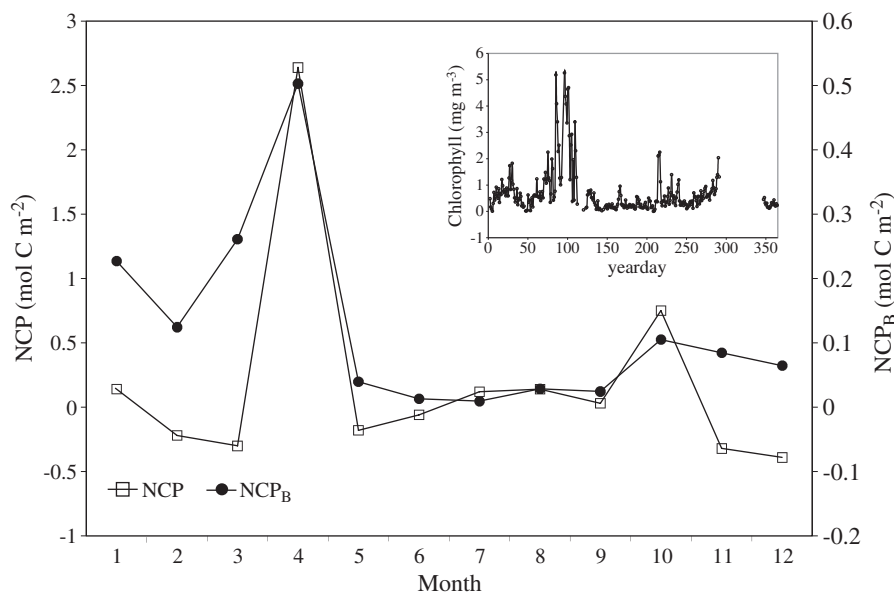


Fig. 16. Monthly values of NCP and NCP_B. Inset: the calibrated time-series of chlorophyll-a fluorescence.

possible sources and sinks, both physical and biological (i.e., advection, vertical diffusion, atmospheric deposition, and nitrification) that will certainly influence the water column NO₃ concentration.

Integrating the monthly estimates of $\Delta\text{DIC}_{\text{bio}}$ and (Jncp), from July to October yielded a post-bloom summer production of 1.0 mol C m^{-2} over the four month period, which corresponds to roughly 40% of the production generated by the spring bloom in April. This production occurred during a period of surface nitrate depletion, and must therefore be fueled by allochthonous nutrients. The POC-based estimate of PP from July to October however yielded a value of $\text{PP}_{\text{SAT}} = 0.58 \text{ mol C m}^{-2}$ over the four month period, which would imply that in the late summer $\text{PP}_{\text{SAT}} < \text{NCP}$. This is due to the fact that this post-bloom production is not accounted for in the (chl-a based) satellite POC estimate of PP, emphasizing the advantage of the DIC based approach (see also Section 5.1).

This summer production, which occurred when the mixed-layer was very shallow, had a large impact on surface water pCO₂. This impact can best be seen in the relationship between the temperature corrected surface pCO₂ and the in-situ water temperature (Fig. 11). After the decay of the spring bloom from June to early September, the surface water warmed from 8 °C to 20 °C. Over the same period, the temperature corrected pCO₂ decreased from roughly 420 μatm (at 8 °C) to less than 300 μatm at the temperature maximum. The summer production resulted in a decrease in pCO₂ of more than 100 μatm. Despite this draw-down, the waters remained supersaturated with respect to atmospheric CO₂ throughout the summer and early autumn due to the effect of temperature on surface pCO₂. The remineralization of the organic matter produced in summer and early autumn increased pCO₂ as the water cooled and the mixed-layer deepened, entraining DIC-rich water from below.

5.2. Trophic status

In autotrophic systems, such as the mixed-layer on the Scotian Shelf, there is a net production of organic matter at the expense of inorganic carbon and nutrients (i.e. $\text{NCP} > 0$). In contrast, heterotrophic systems are defined by a net consumption of organic matter and release of inorganic carbon and nutrients (i.e. $\text{NCP} < 0$). Autotrophic systems may therefore potentially act as sinks of atmospheric CO₂. However, as described above the Scotian Shelf region was found to be a moderate net source of CO₂ to the atmosphere, with an out-gassing of $F = -1.4 \text{ mol C m}^{-2} \text{ yr}^{-1}$, and a reversal of this process occurring only during the

spring bloom. Other regions at similar latitude, with large annual deliveries of fresh water, like the North Sea, and the Baltic Sea, are heterotrophic systems that act as sinks for atmospheric CO₂ (Thomas and Schneider, 1999; Thomas et al., 2005). The Scotian Shelf behaved similarly to an upwelling system, which is often a biologically productive system which releases CO₂ to the atmosphere due to the delivery of DIC-rich waters from below (Lendt et al., 2003; Thomas et al., 2005). The majority of the outgassing of CO₂ on the Scotian Shelf occurred during autumn and winter when the destratification of the water column maintained pCO₂ supersaturation despite the near-zero water temperature. This is in contrast to the interpretation of Chen and Borges (2009) for temperate continental shelves, which on the global scale, tend to act as sinks for CO₂ in the autumn and winter seasons, as in the case of the South and Middle Atlantic Bights (DeGrandpre et al., 2002; Jiang et al., 2008). A recent modeling study (Fennel and Wilkin, 2009) suggests that the continental shelf pump mechanism (Tsunogai et al., 1999) which has the potential to transport DIC-rich water off the shelf and into the adjacent deep ocean does not operate on the Scotian Shelf. Vertical sinking of organic material is insufficient for carbon export since the respiratory products are re-exposed to the surface under conditions of deep winter mixing (Fennel and Wilkin, 2009), the horizontal transport of carbon across the shelf break is not well constrained.

6. Conclusion

Based on highly temporally resolved observations from an autonomous moored instrument, and complementary ship-based sampling over the wider spatial scale, the processes governing the variability of surface pCO₂ and DIC on the Scotian Shelf were evaluated. Biological processes, lateral transport, and entrainment were the dominant factors controlling the variability of mixed-layer DIC. Annual mixed-layer net community production was $\text{NCP} = 2.4 \text{ mol C m}^{-2} \text{ yr}^{-1}$, with a significant portion of this production occurring in summer after the decay of the spring bloom and under nutrient depleted conditions. While the 1-D approach has limitations, particularly with respect to the effect of advection and mixing, this method goes beyond the conventional separation of process into salinity-dependent and salinity-independent variations in DIC allowing the effects of gas exchange, biological processes, vertical entrainment and lateral advection to be examined. This method allows the temporal changes in mixed-layer carbonate system in this coastal system to be understood.

Acknowledgements

We are grateful to the captains, officers and crew of the *CCGS Hudson* for their co-operation in the collection of field data. The authors would like to extend their sincere thanks to K. R. Thompson for his thoughtful comments on the analysis and the manuscript. Many thanks to R. Davis for his assistance with the initial processing of the CARIOCA data, to A. Comeau for the fluorometer calibration, and to D. Worthy at Environment Canada for providing the atmospheric CO₂ data. We are grateful to J. Barthelotte and M. Scotney for the deployment and recovery of the buoy, and to J. Spry and the Bedford Institute of Oceanography for making the archived data from station HL2 accessible. We thank two anonymous reviewers and Nick Bates for their thoughtful and constructive comments. This project was funded by the Canadian Natural Sciences and Engineering Research Council (NSERC) and MetOcean Data Systems, and contributes to IGBP/LOICZ.

References

- Acker, J.G., Leptoukh, G., 2007. Online analysis enhances use of NASA earth science data. *EOS Trans. AGU* 88, 14–17.
- Arrigo, K.R., 2005. Marine microorganisms and global nutrient cycles. *Nature* 437, 349–355.
- Bakker, D.C.E., Etcheto, J., Boutin, J., Merlivat, L., 2001. Variability of surface water f CO₂ during seasonal upwelling in the equatorial Atlantic Ocean as observed by a drifting buoy. *J. Geophys. Res.* 106, 9241–9253.
- Banase, K., 1994. Grazing and zooplankton production as key controls of phytoplankton production in the open ocean. *Oceanography* 7, 13–20.
- Banase, K., 1995. Zooplankton: pivotal role in the control of ocean production. *J. Mar. Sci.* 52, 265–277.
- Bates, N.R., Merlivat, L., Beaumont, L., Pequignet, A.C., 2000. Intercomparison of shipboard and moored CARIOCA buoy seawater fCO₂ measurements in the Sargasso Sea. *Mar. Chem.* 72, 239–255.
- Bates, N.R., Samuels, L., Merlivat, L., 2001. Biogeochemical and physical factors influencing seawater fCO₂ and air–sea CO₂ exchange on the Bermuda coral reef. *Limnol. Oceanogr.* 46, 833–846.
- Bates, N.R., Best, M.H.P., Hansell, D.A., 2005. Spatio-temporal distribution of dissolved inorganic carbon and net community production in the Chukchi and Beaufort Seas. *Deep Sea Res.* 52, 3303–3323.
- Bigelow, H.B., 1927. Physical oceanography of the Gulf of Maine. *Bull. U.S. Bur. Fish.* 640, 511–1027.
- Boehme, S.E., Sabine, C.L., Reimers, C.E., 1998. CO₂ fluxes from a coastal transect: a time-series approach. *Mar. Chem.* 63, 49–67.
- Borges, A.V., Delille, B., Frankignoulle, M., 2005. Budgeting sinks and sources of CO₂ in the coastal ocean: diversity of ecosystems counts. *Geophys. Res. Lett.* 32, L14601.
- Borges, A.V., Tilbrook, B., Metzl, N., Lenton, A., Delille, B., 2008. Inter-annual variability of the carbon dioxide oceanic sink south of Tasmania. *Biogeosciences* 5, 141–155.
- Bozec, Y., Schiettecatte, H.T.L.-S., Borges, A.V., Elkalay, K., de Baar, H.J.W., 2006. Assessment of the processes controlling seasonal variations of dissolved inorganic carbon in the North Sea. *Limnol. Oceanogr.* 51, 2746–2762.
- Brown, C.W., Yoder, J.A., 1993. Blooms of *Emiliania huxleyi* (pymnesiophyceae) in surface waters of the Nova Scotia shelf and Grand Bank. *J. Plankton Res.* 15, 1429–1438.
- Cai, W.-J., Wang, Z.A., Wang, Y., 2003. The role of marsh-dominated heterotrophic continental margins in transport of CO₂ between the atmosphere, the land–sea interface and the ocean. *Geophys. Res. Lett.* 30, 1849.
- Chapman, D.C., Beardsley, R.C., 1989. On the origin of shelf water in the Middle Atlantic Bight. *J. Phys. Oceanogr.* 19, 384–391.
- Chen, C.-T.A., Borges, A.V., 2009. Reconciling opposing views on carbon cycling in the coastal ocean: continental shelves as sinks and near-shore ecosystems as sources of atmospheric CO₂. *Deep Sea Res.* 56, 630–639.
- Chierici, M., Olsen, A., Johannessen, T., Trinanes, J., Wanninkhof, R., 2009. Algorithms to estimate the carbon dioxide uptake in the northern North Atlantic using shipboard observations, satellite and ocean analysis data. *Deep Sea Res.* 56, 630–639.
- DeGrandpre, M.D., Olbu, C.J., Beatty, C.M., Hamar, T.R., 2002. Air–sea CO₂ fluxes on the U.S. Middle Atlantic Bight. *Deep Sea Res.* 49, 4355–4367.
- Dickson, A.G., 1990. Thermodynamics of the dissociation of boric acid in synthetic seawater from 273.15 to 318.15 K. *Deep Sea Res.* 37, 755–766.
- Dickson, A.G., Millero, F.J., 1987. A comparison of the equilibrium constants for the dissociation of carbonic acid in seawater media. *Deep Sea Res.* 34, 1733–1743.
- Droop, M.R., 1973. Some thoughts on nutrient limitation on algae. *J. Phycol.* 9, 264–272.
- Dugdale, R.C., Goering, J.J., 1967. Uptake of new and regenerated forms of nitrogen in primary production. *Limnol. Oceanogr.* 12, 196–206.
- Fennel, K., Wilkin, J., 2009. Quantifying biological carbon export for the northwest North Atlantic continental shelves. *Geophys. Res. Lett.* 36, L18605.
- Fennel, K., Wilkin, J., Levin, J., Moisan, J., O'Reilly, J., Haidvogel, D., 2006. Nitrogen cycling in the Middle Atlantic Bight: results from a three-dimensional model and implications for the North Atlantic nitrogen budget. *Glob. Biogeochem. Cycles* 20, GB3007.
- Fennel, K., Wilkin, J., Previdi, M., Najjar, R., 2008. Denitrification effects on air–sea CO₂ flux in the coastal ocean: simulations for the northwest North Atlantic. *Geophys. Res. Lett.* 35, L24608.
- Fogg, G.E., 1983. The ecological consequence of extracellular products of phytoplankton photosynthesis. *Bot. Mar.* 26, 3–14.
- Fournier, R.O., Marra, J., Bohrer, R., van Det, M., 1977. Plankton dynamics and nutrient enrichment of the Scotian Shelf. *J. Fish. Res. Board Can.* 34, 1004–1018.
- Fransson, A., Chierici, M., Anderson, L.G., Busmann, I., Kattner, G., Jones, E.P., Swift, J.H., 2001. The importance of shelf processes for the modification of chemical constituents in the waters of the Eurasian Arctic Ocean: implication for carbon fluxes. *Cont. Shelf Res.* 21, 225–242.
- Friis, K., Körtzinger, A., Wallace, D.W.R., 2003. The salinity normalization of marine inorganic carbon chemistry data. *Geophys. Res. Lett.* 30, 1085.
- Greenan, B.J.W., Petrie, B.D., Harrison, W.G., Oakey, N.S., 2004. Are the spring and fall blooms on the Scotian Shelf related to short-term physical events. *Cont. Shelf Res.* 24, 603–625.
- Gruber, N., Keeling, C.D., Stocker, T.F., 1998. Carbon-13 constraints on the seasonal inorganic carbon budget at the bats site in the northwestern Sargasso Sea. *Deep Sea Res.* 45, 673–717.
- Hachey, H.B., 1942. The waters of the Scotian Shelf. *J. Fish. Res. Board Can.* 5, 377–397.
- Hannah, C.G., Shore, J.A., Loder, J.W., 2001. Seasonal circulation on the western and central Scotian Shelf. *J. Phys. Oceanogr.* 31, 591–615.
- Hood, E.M., Merlivat, L., 2001. Annual to interannual variations of fCO₂ in the northwestern Mediterranean Sea: results from hourly measurements made by CARIOCA buoys, 1995–1997. *J. Mar. Res.* 59, 113–131.
- Houghton, R.W., Fairbanks, R.G., 2001. Water sources for Georges Bank. *Deep Sea Res.* 48, 95–114.
- Jiang, L.-Q., Cai, W.-J., Wanninkhof, R., Wang, Y., Luger, H., 2008. Air–sea CO₂ fluxes on the U.S. South Atlantic Bight: spatial and seasonal variability. *J. Geophys. Res.* 113, C07019.
- Johnson, K.M., Wills, K.D., Butler, D.B., Johnson, W.K., Wong, C.S., 1993. Coulometric total carbon dioxide analysis for marine studies: maximizing the performance of an automated gas extraction system and coulometric detector. *Mar. Chem.* 44, 167–188.
- Keppay, P.E., Niven, S.E.H., Jellett, J.F., 1997. Colloidal organic carbon and phytoplankton speciation during a coastal bloom. *J. Plankton Res.* 19, 369–389.
- Khatiwala, S.P., Fairbanks, R.G., Houghton, R.W., 1999. Freshwater sources to the coastal ocean off northeastern North America: evidence from H₂¹⁸O/H₂¹⁶O. *J. Geophys. Res.* 104 (18), 241–318 255.
- Kiefer, D.A., 1973. Fluorescence properties of natural phytoplankton populations. *Mar. Biol.* 22, 263–269.
- Lefèvre, N., Aiken, J., Rutllant, J., Daneri, G., Lavender, S., Smyth, T., 2002. Observations of CO₂ in the coastal upwelling off Chile: spatial and temporal extrapolation using satellite data. *J. Geophys. Res.* 107, 3055.
- Lendt, R., Thomas, H., Hupe, A., Ittekkot, V., 2003. Response of the near-surface carbonate system of the northwestern Arabian Sea to the southwest monsoon and related biological forcing. *J. Geophys. Res.* 108, 3222.
- Lewis, E., Wallace, D.W.R., 1998. Program developed for CO₂ systems calculations. ORNL/CDIAC 105, Carbon Dioxide Information Analysis Center, Oak Ridge National Laboratory US Department of Energy, Oak Ridge, Tennessee.
- Loder, J.W., Ross, C.K., Smith, P.C., 1988. A space and time-scale characterization of circulation and mixing over submarine bank with application to the northwestern Atlantic continental shelf. *Can. J. Fish. Aquat. Sci.* 45, 1860.
- Loder, J.W., Han, G., Hannah, C.G., Greenberg, D.A., Smith, P.C., 1997. Hydrography and baroclinic circulation in the Scotian Shelf region: winter versus summer. *Can. J. Fish. Aquat. Sci.* 54.
- Loder, J.W., Petrie, B., Gawarkiewicz, G., 1998. The coastal ocean off northeastern North America: a large-scale view. *The Sea, the Global Coastal Ocean: Regional Studies and Syntheses*. John Wiley, New York, NY, USA.
- Loder, J.W., Hannah, C.G., Petrie, B.D., Gonzalez, E.A., 2003. Hydrographic transport variability on the Halifax section. *J. Geophys. Res.* 108, 8003.
- Mehrbach, C., Culbertson, C.H., Hawley, J.E., Pytkowicz, R.M., 1973. Measurement of the apparent dissociation constants of carbonic acid in seawater at atmospheric pressure. *Limnol. Oceanogr.* 18, 897–907.
- Mills, E.L., Fournier, R.O., 1979. Fish production and the marine ecosystems on the Scotian Shelf, Eastern Canada. *Mar. Biol.* 54, 101–108.
- Mousseau, L., Legendre, L., Fortier, L., 1996. Dynamics of size-fractionated phytoplankton and trophic pathways on the Scotian Shelf and at the shelf break, northwest Atlantic. *Aquat. Microb. Ecol.* 10, 149–163.
- Najjar, R., Butman, D.E., Cai, W.-J., Friedrichs, M.A.M., Kroeger, K.D., Mannino, A., Raymond, P.A., Salisbury, J., Vandemark, D.C., Vlahos, P., 2010. Carbon budget for the continental shelf of the eastern United States: a preliminary synthesis. *Ocean Carbon Biogeochemistry News* 3, 1–4.
- Nightingale, P.D., Malin, G., Law, C.S., Watson, A.J., Liss, P.S., Liddicoat, M.I., Boutin, J., Upstill-Goddard, R.C., 2000. In situ evaluation of the air–sea gas exchange parameterizations using novel conservative and volatile tracers. *Glob. Biogeochem. Cycles* 14, 373–387.
- Olsen, A., Brown, K.R., Chierici, M., Johannessen, T., Neill, C., 2008. Sea-surface CO₂ fugacity in the subpolar North Atlantic. *Biogeosciences* 5, 535–547.
- Omar, A.M., Olsen, A., Johannessen, T., Hoppema, M., Thomas, H., Borges, A.V., 2010. Spatiotemporal variations of fCO₂ in the North Sea. *Ocean Sci.* 6, 77–89.
- Osterroht, C., Thomas, H., 2000. New production enhanced by nutrient supply from non-redfield remineralisation of freshly produced organic matter. *J. Mar. Syst.* 25, 33–46.
- Penn, J.R., 2001. Rivers of the World: A Social, Geographical and Environmental Sourcebook. ABC-CLIO, Inc., Santa Barbara, CA, USA.
- Petrie, B., Smith, P.C., 1977. Low-frequency motions on the Scotian Shelf and slope. *Atmosphere* 15, 117–140.
- Petrie, B., Topliss, B.J., Wright, D.G., 1987. Coastal upwelling and eddy development off Nova Scotia. *J. Geophys. Res.* 92, 12,979–12,991.

- Petrie, B., Drinkwater, K., Gregory, D., Pettipas, R., Sandstöm, A., 1996. Temperature and salinity atlas for the Scotian Shelf and the Gulf of Maine. Canadian Technical Report 171. Hydrography and Ocean Sciences.
- Petrie, B., Yeats, P., Strain, P., 1999. Nitrate, silicate and phosphate atlas for the Scotian Shelf and the Gulf of Maine. Can. Tech. Rep. Hydrogr. Ocean Sci 203.
- Platt, T., Bird, D., Sathyendranath, S., 1991. Critical depth and marine primary production. Proc. R. Soc. Lond. b 246, 205–217.
- Previdi, M., Fennel, K., Wilkin, J., Haidvogel, D., 2009. Interannual variability in atmospheric CO₂ uptake on the northeast U.S. continental shelf. J. Geophys. Res. 114, G04003.
- Redfield, A.C., Ketchum, B.H., Richards, F.A., 1963. The influence of organisms on the composition of sea water v. 2 in The Sea. Interscience.
- Sambrotto, R.N., Savidge, G., Robinson, C., Boyd, P., Takahashi, T., Karl, D.M., Langdon, C., Chipman, D., Marra, J., Codispoti, L., 1993. Elevated consumption of carbon relative to nitrogen in the surface ocean. Nature 363, 248–250.
- Schartau, M., Engel, A., Schröter, J., Thoms, S., Völker, C., Wolf-Gladrow, D., 2007. Modelling carbon overconsumption and the formation of extracellular particulate organic carbon. Biogeosciences 4, 433–454.
- Schiettecatte, L.-S., Gazeau, F., van der Zee, C., Brion, N., Borges, A.V., 2006. Time series of the partial pressure of carbon dioxide (2001–2004) and preliminary inorganic carbon budget in the Scheldt Plume (Belgian coastal waters). Geochem. Geophys. Geosyst. 7, Q096009.
- Schiettecatte, L.-S., Thomas, H., Bozec, Y., Borges, A.V., 2007. High temporal coverage of carbon dioxide measurements in the southern bight of the North Sea. Mar. Chem. 106, 161–173.
- Shadwick, E.H., Thomas, H., Comeau, A., Craig, S.E., Hunt, C.W., Salisbury, J.E., 2010. Air–Sea CO₂ fluxes on the Scotian Shelf: seasonal to multi-annual variability. Biogeosciences 7, 3851–3867.
- Siegel, D.A., Doney, S.C., Yoder, J.A., 2002. The North Atlantic spring phytoplankton bloom and Sverdrup's critical depth hypothesis. Science 296, 730–733.
- Takahashi, T., Sutherland, S.C., Sweeney, C., Poisson, A., Metzl, N., Tilbrook, B., Bates, N.R., Wanninkhof, R., Feely, R.A., Sabine, C.L., Olafsson, J., Nojiri, Y., 2002. Global sea–air CO₂ flux based on climatological surface ocean CO₂, and seasonal biological and temperature effects. Deep Sea Res. II 49, 1601–1622.
- Takahashi, T., Sutherland, S.C., Wanninkhof, R., Sweeney, C., Feely, R.A., Chipman, D.W., Hales, B., Friederich, G., Chavez, F., Sabine, C., Watson, A., Bakker, D.C., Schuster, U., Metzl, N., Yoshikawa-Inoue, H., Ishii, M., Midorikawa, T., Nojiri, Y., Körtzinger, A., Steinhoff, T., Hoppema, M., Olafsson, J., Arnarson, T.S., Tilbrook, B., Johannessen, T., Olsen, A., Bellerby, R., Wong, C., Delille, B., Bates, N., de Baar, H.J., 2009. Climatological mean and decadal changes in surface ocean pCO₂, and net sea–air CO₂ flux over the global oceans. Deep Sea Res. II 56, 554–577.
- Thomas, H., Schneider, B., 1999. The seasonal cycle of carbon dioxide in the Baltic Sea surface waters. J. Mar. Syst. 22, 53–67.
- Thomas, H., Ittekkot, I., Osterroht, C., Schneider, B., 1999. Preferential recycling of nutrients—the ocean's way to increase new production and to pass nutrient limitation? Limnol Oceanogr. 44, 1999–2004.
- Thomas, H., Bozec, Y., Elkalay, K., de Baar, H.J.W., 2004. Enhanced open ocean storage of CO₂ from shelf sea pumping. Science 304, 1005–1008.
- Thomas, H., Bozec, Y., Elkalay, K., de Baar, H.J.W., Borges, A.V., Schiettecatte, L.-S., 2005. Controls of the surface water partial pressure of CO₂ in the North Sea. Biogeosciences 2, 323–334.
- Toggweiler, J.R., 1993. Carbon overconsumption. Nature 363, 210–211.
- Towsend, D.W., Keller, M.D., Holligan, P.M., Ackleson, S.G., Balch, W., 1994. Blooms of the coccolithophore *Emiliania huxleyi* with respect to hydrography in the Gulf of Maine. Cont. Shelf Res. 14, 979–1000.
- Tsunogai, S., Watanabe, S., Sato, T., 1999. Is there a 'continental shelf pump' for the absorption of atmospheric CO₂. Tellus 51, 701–712.
- Umoh, J.U., Thompson, K.R., 1994. Surface heat flux, horizontal advection, and the seasonal evolution of water temperature on the Scotian Shelf. J. Geophys. Res. 99 (20), 403–420 416.
- Walsh, J.J., 1991. Importance of continental margins in the marine biogeochemical cycling of carbon and nitrogen. Nature 350, 753–755.
- Wanninkhof, R., 1992. Relationships between wind speed and gas exchange over the ocean. J. Geophys. Res. 97, 7373–7382.
- Watson, A.J., Schuster, U., Bakker, D.C.E., Bates, N.R., Corbière, A., González-Dávila, M., Friedrich, T., Hauck, J., Heinze, C., Johannessen, T., Körtzinger, A., Metzl, N., Olafsson, J., Olsen, A., Oschlies, A., Padin, X.A., Pfeil, B., Santana-Casiano, J.M., Steinhoff, T., Telszewski, M., Rios, A.F., Wallace, D.W.R., Wanninkhof, R., 2009. Tracking the variable North Atlantic sink for atmospheric CO₂. Science 326, 1391–1393.
- Weiss, R.F., 1974. Carbon dioxide in water and seawater: the solubility of a non-ideal gas. Mar. Chem. 2, 203–215.